University of Szeged
Faculty of Pharmacy
Doctoral School of Pharmaceutical Sciences
Institute of Pharmacognosy

Studies on bioactive 6-gingerol derivatives and thymoquinone-protoflavone hybrid molecules

Ph.D. Thesis

Sara Hassan Hassan Ahmed, M.Sc.

Supervisor:

Attila Hunyadi, D.Sc.

Szeged, Hungary
2024

LIST OF PUBLICATIONS RELATED TO THE THESIS

This thesis is based on the following publications:

I. **Ahmed, S. H. H.**, Gonda, T., Agbadua, O. G., Girst, G., Berkecz, R., Kúsz, N., Tsai, M-C., Wu, C.-C., Balogh, G.T., Hunyadi, A. (2023). Preparation and Evaluation of 6-Gingerol Derivatives as Novel Antioxidants and Antiplatelet Agents
Antioxidants, 12, 744 IF 7.7 (Q1/D1)

II. **Ahmed, S. H. H.**, Bizhar, A. T., Gonda, T., Girst, G., Szőri, K., Berkecz, R., Zupkó, I.**,** Minorics, R., Hunyadi, A. (2024). Preparation of Thymoquinone-Protoflavone Hybrid Molecules as Potential Antitumor Agents.
PLoS ONE, doi: 10.1371/journal.pone.0291567 IF 3.8 (Q1)

Further publications related to the topic of this thesis:

Ahmed, S.H.H., Gonda, T., Hunyadi, A. (2021). Medicinal chemistry inspired by ginger: exploring the chemical space around 6-gingerol.
RSC Advances, 11(43): p. 26687-26699. IF 4.0 (Q1)

Table of Contents

LIST OF ABBREVIATIONS

AA	Arachidonic acid
AAPH	2,2'-Azobis(2-methyl-propionamidine) dihydrochloride
AcN	Acetonitrile
ADME	Adsorption, distribution, metabolism, and elimination
BBB	Blood brain barrier
$CDCl_3$	Deuterated chloroform
CNS MPO	Central nervous system multiparameter optimization
CRC	Colorectal carcinoma
CVDs	Cardiovascular diseases
COX-1	Cyclooxygenase-1 enzyme
DCC	Dicyclohexylcarbodiimide
DMAP	4-Dimethylaminopyridine
DMF	Dimethylformamide
DMSO	Dimethyl sulfoxide
DPPH	1, 1-Diphenyl-2-picrylhydrazyl
FBS	Fetal bovine serum
6-G	6-Gingerol
HPLC	High performance liquid chromatography
LLE	Ligand lipophilic efficiency
MCF-7	Estrogen receptor positive breast cancer cell line
m-CPBA	Meta-chloroperbenzoic acid
MDA	Malondialdehyde
MEM	Minimal essential medium
$ONOO^-$	Peroxynitrite
ORAC	Oxygen radicle absorbance capacity
PA	Protoapigenone
PAMPA	Blood-brain barrier specific parallel artificial membrane permeability assay
PBS	Phosphate buffer saline
PDB	Protein data bank
PIFA	[bis(trifluoroacetoxy)iodo]benzene

PTsOH	p- Toluenesulphonic acid
ROS	Reactive oxygen species
RP-HPLC	Reverse phase high performance liquid chromatography
rt	Room temperature
SAR	Structure-activity relationship
SEM	Standard error of mean
TLC	Thin layer chromatography
TMZ	Temozolomide
TQ	Thymoquinone
WHO	World health organization
XO	Xanthine oxidase

1. INTRODUCTION

Cardiovascular diseases (CVDs) and cancer are currently considered as the first and second leading cause of death; respectively [1, 2]. Despite modern therapeutic options, CVDs are responsible for more than 17 million deaths annually [3]. This urges scientists to continually search for agents that can at least improve the quality of life for patients, even if a complete cure seems hardly achievable.

Great efforts have been devoted toward the discovery of therapeutic agents against these pathologies and many drugs have reached the market, nevertheless, it is still far from reaching the coveted goals.

Nature serves as a great inspiration for drug discovery. The majority of small molecule approved drugs are either natural products or had their origin somehow in nature, either a natural starting material for semi-synthesis or an inspiring natural model compound [4, 5].

One of the drug discovery portals that medicinal chemistry scientists seek is to synthesize derivatives inspired by the structure of natural agents reported to be potentially active against certain diseases. These derivatives are then subjected to bioactivity testing to compare them with the parent compounds and to characterize their pharmacophores [6-9]. *In silico* studies into pharmacokinetics and pharmacodynamics of agents under development also greatly save time and cost invested in drug discovery research [10-13].

This thesis summarizes semi-synthetic work on three natural phenolic compounds: 6-Gingerol (6-G), protoapigenone (PA) and thymoquinone (TQ). Compounds prepared from 6-G were tested for their CVD-related therapeutic potential. Further, the antitumor potential of TQ and PA inspired the preparation of new hybrid compounds containing these two natural products as key building blocks.

2. LITERATURE REVIEW

2.1. Gingerol and its derivatives; isolation, semi-synthesis, and bioactivity

Ginger, *Zingiber officinale* Rosc. (Zingiberaceae), a plant from Asia has been widely used since ancient times as a flavoring spice and a home remedy for many diseases. According to many reports, its root extract proved its effectiveness against a wide spectrum of illnesses [14-17].

Investigations into the chemical composition of ginger root extract revealed a versatile group of constituents. The volatile fraction is composed mainly of sesquiterpene hydrocarbons, mostly zingiberene, curcumin and farnesene, along with monoterpenoid hydrocarbons, the most abundant of which are 1,8-cineole, linalool, geranial, borneol, and neral. Non-volatile constituents of ginger roots are mainly phenolic compounds, among which the gingerols, shogaols, paradols, and zingerone are the most important. Ginger also contains vitamins, organic acids, lipids, and fibers [18, 19].

Ginger phenolics were reported to play a major role in its extracts' bioactivity [19-21]. Different gingerols, which are partially responsible for the pungent flavor of ginger, were isolated from the root extract; the most abundant of which is 6-gingerol [17, 22].

6-Gingerol (6-G), i.e., an aromatic hydrocarbon, (*S*)-5-hydroxy-1-(4-hydroxy-3-methoxy phenyl)decan-3-one (**Fig. 1**), was claimed to possess a wide range of activities [23-33]. The antiplatelet effect of 6-G might be of particular interest since it points out a potential role in cardiovascular disease (CVD) prevention and/or treatment [30, 31].

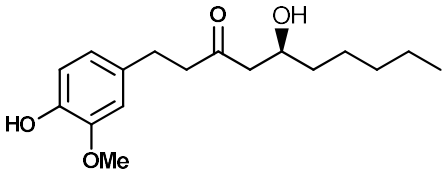

Figure (1): The structure of 6-Gingerol (**1**)

The possibility for the use of ginger extract as a supportive measure in CVDs was reported [16, 34]. Some studies proposed that this effect might be due to the inhibition of platelet aggregation [15, 35-38], which in turn suggested being mediated through interfering with Cyclooxygenase-1 (COX-1) enzymatic function and reactive oxygen species formation [34, 39]. Inhibition of AA-induced platelet aggregation by an aqueous ginger extract was investigated. A reduction in thromboxane formation was noted which was suggested to be mediated via the inhibition of COX-1 enzyme activity [40]. The impact of ginger consumption on platelet aggregation and coagulation was also clinically investigated in healthy volunteers, and no effects were observed [41, 42]. However, the consumption of ginger in combination with nifedipine was found to potentiate its antiplatelet effects on patients with coronary artery disease [43]. Isolated 6-G was also studied against CVDs and promising results were reported [44-47].COX-1 enzyme, also known as the prostaglandin G/H synthase or prostaglandin-endoperoxide synthase (PTGS), is expressed constitutively in all tissues and controls the production of prostanoids [48]. It is a homodimer integral membrane protein and a bifunctional enzyme with cyclooxygenase and peroxidase functionality. It converts free arachidonic acid (AA) into prostaglandin H2 (PGH2); which in turn is converted to thromboxane A2 (TXA2) in platelets via thromboxane A2 synthase enzyme. TXA2 is an inducer of platelet activation and aggregation. Increased levels of TXA2 may play a role in atherosclerosis, stroke, myocardial infarction, pulmonary hypertension, and even angiogenesis and metastasis in cancer [49].

The crystal structure of *h*-COX-1 (PDB: 6Y3C) was recently revealed by Miciaccia et al. [50], before this, the crystallographic data for ovine COX-1 isoenzyme were available [51, 52]. COX-1 is a homodimer, with three structural domains for each monomer: a C-terminal catalytic domain, a membrane binding domain, and a short N-terminal epidermal growth factor domain. The first domain contains the peroxidase (POX) and the COX active sites, they are positioned opposite to each other with the heme prosthetic group located at the base of the former [50, 53].

Studies revealed the identity of some key amino acids present in the COX active site, which may play a crucial role in the process of binding to the substrates e.g., S350, Y385, I523, V349,

and W387. The amino acids R120, Y355, and E524 form an H-bonding network that allows for a constriction at the base of the active site [50, 54], The channel at the top of the active site contains the amino acid G533 which was considered to be important for the AA-oxidation. This was confirmed via mutagenesis studies. Replacing bulky substituents at this position inhibited the AA-oxidation process [55]. Similarly, R120 mutagenesis was reported to render the enzyme resistant to inhibition by substrates [54].

As mentioned earlier, platelet activation could also be influenced by high reactive oxygen species (ROS) levels [39]. The antioxidant activity of ginger extract and 6-G was well investigated [16, 26, 56, 57]. A study reported that feeding of 1% ginger to malathion-treated rats for four weeks significantly attenuated oxidative stress and lipid peroxidation induced by malathion, and, remarkably, this was as effective as ascorbic acid treatment [34]. 6-G was reported to protect cardiac tissues against alcohol-induced ROS-mediated damage in rats fed with an alcohol/6-G mixed diet [58], and to prevent hypoxia-induced cardiomyocyte injury, which was attributed to its antioxidant effects [59]. It also reduced hydrogen peroxide-induced oxidative stress and cellular death in zebrafish [60].

Tremendous efforts were dedicated to the synthesis of derivatives out of 6-G for further potential bioactivity testing. So far, over 150 compounds have been synthesized and tested as we have recently reviewed [61]. Our in-depth literature survey led us to the conclusion that the antiplatelet activity might be the most promising for this group of compounds [62, 63]; gingerol derivatives that were studied for their antiplatelet properties are shown in **Fig. 2**.

Shih et al. reported the synthesis and antiplatelet-aggregation testing of 6-G (**1**) and other (natural/ synthetic) derivatives (**Fig. 2**; compounds **2–15** and **17–47**). Compounds of the paradol series were the most active, especially 6-paradol (**7**) (IC_{50} = 0.070 μg/mL compared to 1 μg/mL for 6-G). The introduction of a double bond or a hydroxyl group at the β-position resulted in a reduction in the activity, however, increasing the alkyl side chain length increased it (e.g. the dehydroparadol compound **40** showed an IC_{50} value of 0.160 μg/mL). The epoxide derivatives (**41**–**46**) showed a lower potency compared to *n*-paradols (IC_{50} = 0.96–2.38 μg/mL) [62]. Koo et al. investigated the effect of 6-G (**1**) and its synthetic analogues (**Fig. 2**; compounds **3**, **48**, **49**, **52**, **54** and **55**) on the AA-induced platelet serotonin release and aggregation, a lower platelet aggregation inhibitory activity for all compounds (IC_{max} = 10–25 μM) as compared to acetylsalicylic acid (IC_{max} = 6 μM) was noted. To examine the underlying mechanism, COX-inhibitory activity was studied. Compounds **55**, **3**, and **54** induced similarly potent inhibitory activity (IC_{50} = 1.2, 1.5, and 3.3 μM, respectively) as the positive control indomethacin (IC_{50} = 0.76 μM), compared to 50 μM for 6-G (**1**). Notably, their COX inhibitory activity correlated with their hydrophobicity, with compound **55** being the most active and the most hydrophobic at the same time [63].

The anti-platelet and COX-1 inhibitory activity were also assessed for another set of gingerol derivatives (**Fig. 2**; compounds **2**–**4**, **7**-**9**, **12**, **16**, **50**, **51** and **53**–**61**). 8-Paradol (**8**) was reported as the most promising among all (75% inhibition at 2 μM compared to 3.4% for 6-G (**1**) at the same concentration). Studies into the SAR highlighted the importance of the carbonyl function

at C3 for activity, any other substituents on the alkyl chain interfere with the activity. This was obvious through comparison of compound **8** and compound **57** activity (IC_{50} = 20 μM) [158].

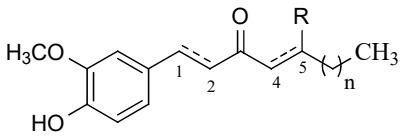

	R	n	1,2-bond	4,5-bond
2	H	4	$\sigma^{1,2}$	$\Delta^{4,5}$
3	OH	6	$\sigma^{1,2}$	$\sigma^{4,5}$
4	OH	8	$\sigma^{1,2}$	$\sigma^{4,5}$
5	OH	4	$\Delta^{1,2}$	$\sigma^{4,5}$
6	H	4	$\Delta^{1,2}$	$\Delta^{4,5}$
7	H	4	$\sigma^{1,2}$	$\sigma^{4,5}$
8	H	6	$\sigma^{1,2}$	$\sigma^{4,5}$
9	H	6	$\sigma^{1,2}$	$\Delta^{4,5}$
10	OH	3	$\sigma^{1,2}$	$\sigma^{4,5}$
11	OH	5	$\sigma^{1,2}$	$\sigma^{4,5}$
12	OH	7	$\sigma^{1,2}$	$\sigma^{4,5}$
13	OH	6	$\Delta^{1,2}$	$\sigma^{4,5}$
14	H	4	$\Delta^{1,2}$	$\sigma^{4,5}$
15	H	6	$\Delta^{1,2}$	$\sigma^{4,5}$
16	OH	10	$\sigma^{1,2}$	$\sigma^{4,5}$
17	OH	3	$\Delta^{1,2}$	$\Delta^{4,5}$
18	OH	5	$\Delta^{1,2}$	$\Delta^{4,5}$
19	OH	7	$\Delta^{1,2}$	$\Delta^{4,5}$
20	H	3	$\Delta^{1,2}$	$\Delta^{4,5}$
21	H	5	$\Delta^{1,2}$	$\Delta^{4,5}$
22	H	6	$\Delta^{1,2}$	$\Delta^{4,5}$
23	H	7	$\Delta^{1,2}$	$\Delta^{4,5}$
24	H	8	$\Delta^{1,2}$	$\Delta^{4,5}$
25	OH	3	$\Delta^{1,2}$	$\sigma^{4,5}$
26	OH	5	$\Delta^{1,2}$	$\sigma^{4,5}$
27	OH	7	$\Delta^{1,2}$	$\sigma^{4,5}$
28	OH	8	$\Delta^{1,2}$	$\sigma^{4,5}$
29	H	3	$\sigma^{1,2}$	$\Delta^{4,5}$
30	H	5	$\sigma^{1,2}$	$\Delta^{4,5}$
31	H	7	$\sigma^{1,2}$	$\Delta^{4,5}$
32	H	8	$\sigma^{1,2}$	$\Delta^{4,5}$
33	H	3	$\sigma^{1,2}$	$\sigma^{4,5}$
34	H	5	$\sigma^{1,2}$	$\sigma^{4,5}$
35	H	7	$\sigma^{1,2}$	$\sigma^{4,5}$
36	H	8	$\sigma^{1,2}$	$\sigma^{4,5}$
37	H	3	$\Delta^{1,2}$	$\sigma^{4,5}$
38	H	5	$\Delta^{1,2}$	$\sigma^{4,5}$
39	H	7	$\Delta^{1,2}$	$\sigma^{4,5}$
40	H	8	$\Delta^{1,2}$	$\sigma^{4,5}$

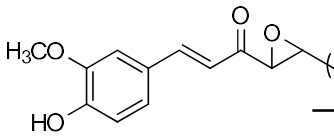

	n
41	3
42	4
43	5
44	6
45	7
46	8

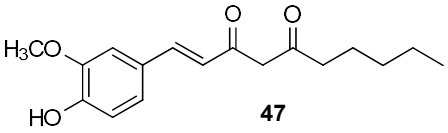

47

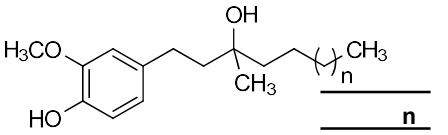

	n
48	5
49	7

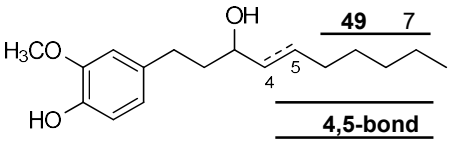

	4,5-bond
50	$\Delta^{4,5}$
51	$\sigma^{4,5}$

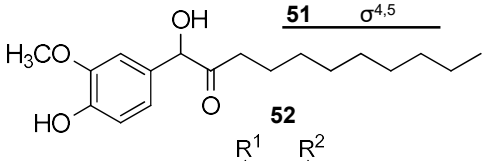

52

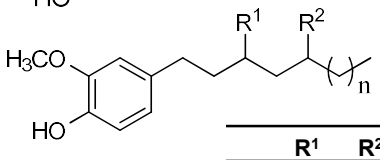

	R¹	R²	n
53	OH	OH	4
54	OH	OH	6
55	OH	H	6
56	H	OH	6

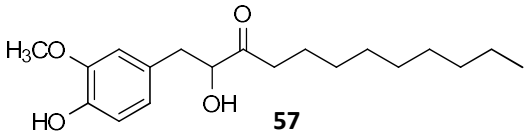

57

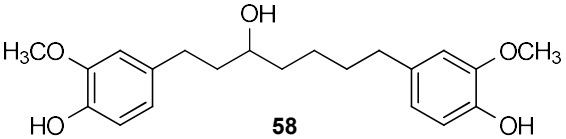

58

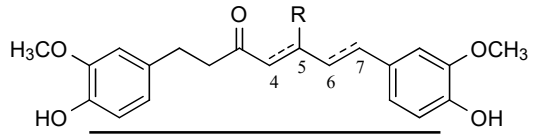

	R	4,5-bond	6,7-bond
59	H	$\sigma^{4,5}$	$\sigma^{6,7}$
60	OH	$\sigma^{4,5}$	$\Delta^{6,7}$
61	H	$\Delta^{4,5}$	$\Delta^{6,7}$

Figure 2. Gingerol derivatives with *in vitro* anti-platelet activity

2.2. Protoflavones, thymoquinone, and their hybrid molecules with antitumor properties

Among the different types of cancer, breast cancer is ranked the second leading cause of cancer death among women after lung cancer in western countries in 2022 [64], whereas, cervical cancer represents the fourth most common cancer type in women with more than 600,000 new cases recorded only in 2020 [65]. Glioblastoma is another very challenging type of cancer that occurs in the brain or the spinal cord. It is the most common and devastating brain tumor in adults. Different treatment modalities are adopted in cancer management, from chemotherapy, and radiotherapy to surgical intervention [66]. A great body of phytochemicals-based cancer-related research has been conducted [67-72]. Among these is the research on *Thelypteris torresiana* and *Nigella sativa* and their constituents.

2.2.1. Antitumor potential of protoapigenone and its derivatives

Extracts of *Thelypteris torresiana* Gaud. (Thelypteridaceae), a fern native to Taiwan, were studied against different kinds of cancer and encouraging results were obtained [73]. A group of compounds was isolated from the whole plant including flavonoids, phenols, sesquiterpenes, and steroids [74]. Protoapigenone (PA); 5,7-dihydroxy-2-(1-hydroxy-4-oxocyclohexa-2,5-dien-1-yl) chromen-4-one (**Fig. 3**), a rare protoflavone from this plant was identified as the main active constituent responsible for its anti-cancer potential [73]. This flavonoid has a very characteristic unusual *p*-quinol B-ring that was described as the main pharmacophore [75]. Hunyadi et al. reported the first semisynthetic preparation of PA from apigenin, and identified new structure-activity relationships concerning the 1'-*O*-alkyl substituents [76].

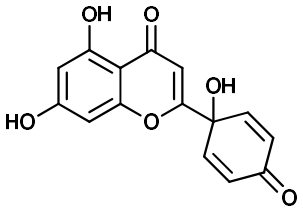

Figure (3): The structure of protoapigenone (**62**)

PA has been studied against different types of cancer and different mechanisms of action have been suggested [76-82]. It may be of particular interest that it inhibits the ATR-dependent phosphorylation of Chk1 kinase, a key step of DNA damage response (DDR) signaling [83]. PA also promoted apoptosis of MDAH-2774 cell line and induced cell cycle arrest [77]. The induction of apoptosis was related to the activation of p38 mitogen-activated protein kinase and c-Jun NH_2-Terminal Kinase (JNK) in prostate cancer cell lines [84]. PA was also found to inactivate the PIK3/AKT1 signaling pathway in cervical cancer cells [79]. Its cell cycle arrest and apoptosis-inducing effects were proposed to be oxidative stress-mediated [77, 84-86]. PA is studied in many currently ongoing clinical trials, e.g., NCT02487095, NCT04616534, NCT04802174, NCT05338346, etc.

Several studies aimed to synthesize new antitumor agents inspired by PA. WYC0209, a synthetic PA analog, exerted much stronger antitumor effects than its parent compound; it reduced the viability and growth of urothelial cancer cell lines in a dose-dependent manner by

interfering with the cell cycle and enhancing apoptotic cellular death [87]. It also induced apoptosis and inhibited cellular proliferation of colorectal carcinoma (CRC) [88], and prostate cancer cell lines [86]. RY10-4, a synthetic analog possessing the minimum pharmacophore of PA, showed enhanced activity against breast, ovarian, prostate, liver, and pancreatic cancer cell lines compared to PA [89]. Different mechanistic pathways were deciphered for this compound, e.g., the downregulation of P-gp expression [90], induction of autophagy [91] and apoptosis [92, 93], and the suppression of angiogenesis [94] and metastasis in breast cancer cell lines [95]. It was also claimed to be effective against the human lung adenocarcinoma A549 cell line [96].

2.2.2. Antitumor potential of thymoquinone

Nigella sativa L. (Ranunculaceae), commonly known as black seed or black cumin, is widely consumed for food seasoning and medicinal purposes. It is grown in western Asia, eastern Africa, and the middle east. It has been widely used for the treatment of headache, as an analgesic and diuretic, and against skin and gastrointestinal disorders. Its biological activity was attributed to the main constituent in its essential oil, the monoterpene thymoquinone [97-99]. The seeds contain many other bioactive compounds including thymohydroquinone, dithymoquinone, carvacrol, *t*-anethol, 4-terpineol, α-pinene, *p*-cymene, and thymol [98].

Thymoquinone (TQ); 2-methyl-5-propan-2-ylcyclohexa-2,5-diene-1,4-dione (**Fig. 4**); was described to possess a wide array of bioactivities including antioxidant, anti-inflammatory, antimicrobial, immunomodulatory, neuromodulatory, and anticancer activities [100-108]. Encouraging results were reported against many cancer types, such as colorectal carcinoma, squamous cell carcinoma, prostate cancer, colon cancer, myeloblastic anemia, and fibrosarcoma [109]. TQ was also claimed to potentiate the effect of existing chemotherapeutics [99], and to provide protective effects against their toxicities [101, 105, 110]. A sensitizing effect to radiotherapy was also reported [111], while it was found to be safe in many normal cell lines [112-114].

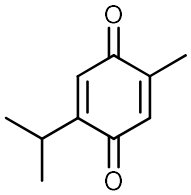

Figure (4): The structure of Thymoquinone (**63**)

TQ was studied against different types of cancer and different mechanistic pathways were suggested. It was proposed to affect multiple signaling pathways, such as nuclear factor kappa-β (NF-κβ), phosphatidylinositol-4,5-bisphosphate 3-kinase (PI3K)/serine/ threonine-specific protein kinase B (AKT), mitogen-activated protein kinase (MAPK), signal transducer and activator of transcription (STAT), eukaryotic elongation factor 2 kinase (eEF-2 K), and p53 signaling pathways, thus, influencing cancer cells proliferation, metastasis, and angiogenesis. It also influenced the cell cycle progression by regulating miRNAs expression [97, 115-117]. Furthermore, TQ induced apoptosis via p53-independent pathways in p53-null myeloblastic leukemia HL-60 cells [109]. Its combination with doxorubicin was found to increase the

Bax/Bcl2 ratio, and to subsequently promote apoptosis in doxorubicin-induced senescent and proliferative breast and colon cancer cells [118]. The prooxidant-antioxidant properties of TQ were also studied. Its effects on apoptotic genes were correlated to the enhancement of cellular malondialdehyde (MDA), reactive oxygen species (ROS), and nitric oxide (NO) levels in MDA-MB-231 cell lines [119]. Likewise, it increased ROS levels in pancreatic cancer cell lines [120].

TQ was also studied against glioblastoma. It exerted selective toxicity against glioblastoma cells compared to primary astrocytes, besides its ability to cross the BBB. It was reported to affect cellular redox state and mitochondrial function leading to cell cycle arrest and apoptosis [121], inhibit telomerase activity leading to telomere attrition and DNA damage [113], and inhibit autophagy and induce a caspase-independent glioblastoma cells death [122]. It reduced the migration and invasiveness of glioblastoma cells through the downregulation of the Focal Adhesion Kinase (FAK) protein [123], and potentiated the effects of temozolomide [124, 125]. Even in TMZ-resistant glioblastoma cells, it induced apoptosis via P38-mitogen activated protein kinase signaling pathway [126]. Several derivatives were synthesized based on the structure of TQ, and many showed effectiveness against different types of cancer cell lines. TQFL12, an aromatic imine derivative of TQ, demonstrated superior antiproliferative effects on TNBC cells compared to the parent molecule [127].

2.2.3. Hybrid compounds previously prepared using thymoquinone or protoflavones

The field of drug discovery has witnessed an increasing popularity of molecular hybridization as a rational drug design approach. It means designing new molecules that are based on fragments of known, complementary bioactivities and joining them into a hybrid molecule through linkers or direct fusion. This aims for multitarget candidates that may simultaneously exploit the synergistic bioactivities of its fragments. This approach may especially be promising in combating diseases of multifactorial nature like cancer [128-130]. Such molecules might have a bioactivity superior to their building blocks and may offer new ways to overcome drug resistance [131-133]. Our group previously reported the preparation of two series of antitumor hybrids containing a protoflavone fragment. Natural, or semi-synthetic protoflavonoids were linked to chalcone [134] or indole derivatives [135]. In both series, a protoflavone fragment was included as an ATR signaling inhibitor, and it was combined either with an oxidative stress inducing fragment (i.e., a ferrocene or a chalcone), or with an activator of p53 (i.e., a spiropyrazole oxindole). Both hybrid compound series demonstrated greatly improved efficacy against breast cancer cell lines.

Some synthetic efforts were also dedicated to preparing hybrid compounds based on TQ. It was combined with 5-fluorouracil into hybrid structures using different linkers, and this resulted in molecules that are active against CRC cell lines [136]. TQ was also combined with artemisinin into hybrid molecules, among which a TQ-artesunic acid hybrid was the most effective (IC_{50} of 2.4 μM) in CRC cell line, being up to 20 folds more active than the parent compounds [137].

3. OBJECTIVES

In this PhD work, it was our main objective to prepare and study natural phenolic compounds and their semi- or total synthetic derivatives, and to evaluate their bioactivities. Two distinct groups of target compounds and bioactivity profiles were targeted, according to the following.

3.1. 6-Gingerol derivatives

Inspired by the antiplatelet activity of 6-gingerol and its derivatives, in this part of the work we aimed to

1. synthesize, purify, and characterize semi- or total synthetic derivatives of 6-G, and
2. in research collaboration, to study their AA-induced platelet aggregation inhibitory activity, COX-1 enzyme inhibitory activity, and antioxidant activity, and to assess their ADME behavior using experimental and *in silico* tools, and
3. to predict their interaction with *h*-COX-1 enzyme utilizing *in silico* molecular docking.

3.2. Thymoquinone-protoflavone hybrids

Inspired by the antitumor activity of protoflavones and thymoquinone, their ability to interfere with DNA damage response signaling at different levels, and the previous work reported on hybrid compounds containing either of these compounds, in this part of the work we aimed to

1. combine TQ with different protoflavone derivatives into ester-linked hybrid structures,
2. in research collaboration, to assess the antiproliferative potentials of these compounds together with their parent fragments (alone and in combination) against gynecological and glioblastoma cell lines, and
3. to evaluate structure-activity relationships and interpret bioactivity data in view of the compounds' chemical stability.

4. MATERIALS AND METHODS

4.1. General information

Reagents were purchased from Sigma (Merck KGaA, Darmstadt, Germany) unless otherwise stated. Solvents (analytical grade for synthetic work and flash chromatography purifications and high-performance liquid chromatography (HPLC)-grade for analytical and preparative HPLC work) were obtained from Macron Fine Chemicals (Avantor Performance Materials, Center Valley, PA, USA), Chem-Lab NV (Zedelgem, Belgium), VWR International S.A.S., and Fontenay-sous-Bois, France. A commercial ginger extract was purchased from Xi'an Pincredit Bio-Tech Co., Ltd., China. COX-1 kit was obtained from VWR International Kft. Debrecen, Hungary (original source: Biovision Inc., Milpitas, CA, USA). For purification of the compounds, flash chromatography was used on a CombiFlashfi Rf+ Lumen apparatus (TELEDYNE Isco, Lincoln, NE, USA) equipped with evaporative light scattering (ELS) and diode array detectors, and the stationary phases were RediSep prefilled silica columns and RediSep cartridges (Teledyne Isco Inc., Lincoln, NE, USA).

Hereinafter, solvent system compositions are always given in volumetric ratios. Preparative purifications over RP-HPLC were performed on a Kinetex XB C18 (5 μm, 250 × 21.2 mm) column on an Armen Spot Prep II integrated HPLC purification system (Gilson, Middleton, WI, USA) with dual-wavelength detection, with an adequately chosen combination of acetonitrile and water, and a flow rate of 15 mL/min. Semi-preparative purification was performed on an Agilent 1100 series (Waters Co., Milford, MA, USA) connected to a Jasco UV-2075 detector (Jasco Co., Tokyo, Japan) utilizing a C18 column (5 μm, 250 x 10 mm) with a flow rate of 3 mL/min. The purity of the compounds obtained was determined by RP-HPLC analyses on a system of two Jasco PU 2080 pumps, a Jasco AS-2055 Plus intelligent sampler connected to a JASCO LC-Net II/ADC equipped with a Jasco MD-2010 Plus PDA detector (Jasco International Co. Ltd., Hachioji, Tokyo, Japan) utilizing a Kinetex C-18 (5 μm, 250 × 4.6 mm) column (Phenomenex Inc., Torrance, CA, USA) and applying a gradient of 30%–100% aqueous AcN in 30 min followed by 100% AcN for 10 min with a flow rate of 1 mL/min. Analysis of samples from the PAMPA and kinetic solubility assays was performed the same way, by using 3-point calibrations and integrating each compound at its UV absorption maximum.

^{1}H- and ^{13}C NMR spectra were recorded in $CDCl_3$ or CD_3OD using 5 mm tubes at room temperature on a Bruker DRX-500 spectrometer at 500 (^{1}H) and 125 (^{13}C) MHz with the deuterated solvents' signal taken as reference. The heteronuclear single quantum coherence (HSQC), heteronuclear multiple bond correlation (HMBC), ^{1}H-^{1}H correlation spectroscopy (COSY), and nuclear Overhauser effect spectroscopy (NOESY) spectra were obtained using the standard Bruker pulse programs. High resolution mass spectroscopy (HRMS) spectra were recorded on a Q-Exactive Plus hybrid quadrupole-orbitrap mass spectrometer (Thermo Scientific, Waltham, MA, USA) equipped with heated electrospray ionisation (HESI-II) probe that was used in positive or negative mode per needed.

All bioactivity data processing, including the calculation of inhibition percentage, mean and corresponding standard error of the mean (SEM), and IC_{50} values, was performed by GraphPad Prism 8.0 or 9.5.1 (GraphPad Software, San Diego, CA, USA) (La Jolla, CA, USA). IC_{50} values were calculated from the sigmoidal dose–response curves obtained by the log(inhibitor) vs. response and variable slope (DPPH assay) or the log(inhibitor) vs. normalised response and variable slope nonlinear regression model. For the gingerols work, no statistical evaluation was performed on the results obtained; instead, differences greater than two-fold were considered relevant. Plotting of the antiplatelet and COX-1 inhibitory IC_{50} values and the linear regression of the data was performed by Microsoft Excel, while GraphPad was used for the hybrids.4.2. 6-Gingerol derivatives; isolation, synthesis, and testing

4.2.1. Isolation and synthesis

4.2.1.1. Purification of 6-gingerol ((*S*)-5-hydroxy-1-(4-hydroxy-3-methoxyphenyl) decan-3-one) (1)

Ginger extract was purchased from Xi'an Pincredit Bio-Tech Co., Ltd., Xi'an, China. 6-G (**1**) was purified from the crude extract at up to a 4 g scale using flash chromatography (Silica,

gradient elution of 0–10% of acetone in *n*-hexane) and obtained as a dark yellow oil (36.8% yield). 6-G (**1**) was then utilised to synthesize 6-shogaol (**2**), and subsequently 4,5-dihydro-6-shogaol (**7**), as published previously [138]. Compound **47** was derived from vanillin (**67**) and 2,4-nonanedione (**70**), and compound **72** from compound **47**, as published previously [139].

4.2.1.2. Synthesis of 1-(4-hydroxy-3-methoxyphenyl)decan-3-one oxime (64)

Hydroxylamine hydrochloride (228 mg, 3.3 mmol) was added to a solution of compound **7** (304 mg, 1.1 mmol) in MeOH (5 mL) at room temperature. The reaction was monitored by thin-layer chromatography (TLC), the reaction mixture was purified by flash chromatography (Silica, gradient elution of 0–30% of EtOAc in *n*-hexane) to afford compound **64**, a pale-yellow solid (255 mg, 74.8%) [140].

Compound 64. HRESIMS: $C_{17}H_{27}NO_3$, $[M+H]^+$ *m/z* = 294.20694 (calcd 294.20692), ^{1}H NMR (500 MHz, in $CDCl_3$): δ_H 6.83 (m, 1H), 6.70 (dd, 2H, *J* = 13.8, 7.6 Hz), 3.88 (d, 3H, *J* = 3.5 Hz), 3.48 (s, 1H), 2.77 (q, 2H, *J* = 8.0 Hz), 2.60 (m, 1H), 2.46 (m, 1H), 2.36 (m, 1H), 2.10 (t, 1H, *J* = 7.6 Hz), 1.50 (m, 2H), 1.31 (m, 2H), 1.28 (m, 7H), 0.88 (td, 3H, *J* = 7.0, 2.9 Hz) ppm. ^{13}C NMR (125 MHz, in $CDCl_3$): δ_C 161.8, 161.7, 146.6, 144.1, 144.0, 133.6, 133.4, 121.0, 114.5, 111.1, 56.1, 36.4, 34.6, 32.5, 31. 9, 31.9, 31.5, 30.0, 30.0, 29.4, 29.2, 27.9, 26.4, 25.8, 22.8, 14.2.

4.2.1.3. Synthesis of (3*R*,5*S*)-1-(4-hydroxy-3-methoxyphenyl)decane-3,5-diol (65) and (3*S*,5*S*)-1-(4-hydroxy-3-methoxy phenyl)decane-3,5-diol (66)

Compound **1** (100 mg, 0.34 mmol) was dissolved in EtOH (10 mL) and $NaBH_4$ was added (38 mg, 1 mmol). The reaction was monitored by means of TLC and after completion (1 h) the solvent was evaporated in vacuo and water (20 mL) was added to the residue. The aqueous phase was extracted with EtOAc (3 × 20 mL), and the combined organic phase was dried over Na_2SO_4, filtered, and evaporated in vacuo resulting in a yellow oil (85 mg, 84%), which contained the gingerdiols in high purity (>95%), which were separated via preparative HPLC (50% aqueous AcN) to yield compound **65** as a faint yellow oil, and compound **66** as a white powder. The compounds' MS and NMR spectra were in good agreement with the literature data [141].

4.2.1.4. Synthesis of (*E*)-1-(4-hydroxyphenyl)dec-1-ene-3,5-dione (71)

p-Hydroxybenzaldehyde **68** (1000 mg, 8.2 mmol), boron trioxide (2280 mg, 32.8 mmol), and 2,4-nonanedione **70** (2800 mg, 24.6 mmol) were mixed with 2 mL of DMF and heated to 90 °C. A solution of isobutylamine (150 mg = 202 µL, 4 mmol) in 2 mL of DMF was added dropwise over 2 h. The reaction mixture was stirred at 90 °C for 1 h then 50 mL of water was added. The resulting mixture was stirred at 60 °C for 1 h at room temperature overnight. The reaction mixture was extracted with EtOAc and the solvent was evaporated. Purification by flash chromatography (Silica, gradient elution, 5–10% EtOAc in *n*-hexane) afforded compound **71**, a yellow solid (179 mg, 8.5%) [139].

Compound 71. HRESIMS: $C_{16}H_{20}O_3$, $[M\text{-}H]^-$ *m/z* = 259.1332, (calcd 260.13342), ^{1}H NMR (500 MHz, in CD_3OD): δ_H 7.57 (d, 1H, *J* = 15.9 Hz), 7.50 (d, 2H, *J* = 8.6 Hz), 6.84 (m, 2H), 6.51 (d, 1H, *J* = 15.9 Hz), 2.42 (m, 2H), 1.67 (p, 2H, *J* = 7.7, 7.3 Hz), 1.39 (m, 4H), 0.97 (t, 3H, *J* = 7.0 Hz) ppm. ^{13}C NMR (125 MHz, in CD_3OD): δ_C 201.6, 179.6, 160.9, 141.3, 2 × 131.0, 128.1, 120.6, 2 ×116.9, 44.3, 40.9, 32.6, 26.5, 23.5, 14.3.

4.2.1.5. Synthesis of 2-methoxy-4-(2-(3-pentyl-1H-pyrazol-5-yl)ethyl)phenol (73), 4-(2-(3-pentyl-1H-pyrazol-5-yl)ethyl)phenol (74), and (E)-4-(2-(3-pentyl-1H-pyrazol-5 yl)vinyl) phenol (75)

To a stirred solution of compounds **47** or **71** (164 mg, 0.57 mmol/100 mg, 0. 38 mmol) in ethanol (2 mL), hydrazine monohydrate (71 mg = 71 µL, 1.4 mmol/134 mg = 48 µL, 2.67 mmol) and a catalytic amount of concentrated HCl were added. The reaction mixture was refluxed for 6 h, cooled to ambient temperature, evaporated in vacuo, and purified using preparative HPLC (AcN: H_2O 40:60 for compound **73** and 42:58 for **74** and **75**) to afford compounds **73** (270 mg, 17.8%), **74**, (22 mg, 22.3%) or **75**, (23 mg, 23.6%) as pale-yellow solids [142].

Compound 73. HRESIMS: $C_{17}H_{24}N_2O_2$, $[M+H]^+$ *m/z* = 289.19111 (calcd 289.19160). ^{1}H NMR ($CDCl_3$, 500 MHz): δ_H 6.83 (d, 1H, *J* = 8.0 Hz), 6.70 (dd, 1H, *J* = 8.0, 2.0 Hz), 6.67 (d, 1H, *J* = 2.0 Hz), 5.84 (s, 1H), 3.84 (s, 3H), 3.48 (s, 1H), 2.89 (m, 4H), 2.59 (t, 2H, *J* = 7.7 Hz), 1.64 (m, 2H), 1.35 (m, 2H), 1.33 (m, 2H), 0.90 (t, 3H, *J* = 7.1 Hz) ppm. ^{13}C NMR (125 MHz, in $CDCl_3$): δ_C 146.6, 144.2, 133.6, 121.2, 114.5, 111.3, 102.6, 56.1, 35.6, 31.7, 29.6, 29.2, 27.0, 22.6, 14.1.

Compound 74. HRESIMS: $C_{16}H_{22}N_2O$, $[M+H]^+$ *m/z* = 259.18057 (calcd 259.18104), ^{1}H NMR (500 MHz, in $CDCl_3$): δ_H 6.99 (d, 2H, *J* = 8.4 Hz), 6.71 (d, 2H, *J* = 8.5 Hz), 5.86 (s, 1H), 3.48 (s, 1H), 2.88 (t, 2H, *J* = 3.9 Hz), 2.87 (t, 2H, *J* = 4.2 Hz), 2.59 (t, 2H, *J* = 7.7 Hz), 1.63 (m, 2H), 1.34 (m, 2H), 1.31 (t, 2H, *J* = 3.9 Hz), 0.90 (t, 3H, *J* = 7.1 Hz) ppm. ^{13}C NMR (125 MHz, in $CDCl_3$): δ_C 154.7, 149.4, 148.9, 133.1, 2 × 129.6, 2 × 115.6, 102.6, 34.9, 31.6, 29.3, 29.1, 27.1, 22.6, 14.1.

Compound 75. HRESIMS: $C1_6H_{20}N_2O$, $[M+H]^+$ *m/z* = 257.16489 (calcd 257.16539), ^{1}H NMR (500 MHz, in CD_3OD): δ_H 7.34 (d, 2H, *J* = 8.6 Hz), 7.01 (d, 1H, *J* = 16.5 Hz), 6.85 (d, 1H, *J* = 16.5 Hz), 6.77 (d, 2H, *J* = 8.6Hz), 6.24 (s, 1H), 2.62 (t, 2H, *J* = 7.6 Hz), 1.67 (m, 2H), 1.38 (m, 2H), 1.36 (m, 2H), 0.92 (t, 3H, *J* = 6.8 Hz) ppm. ^{13}C NMR (125 MHz, in CD_3OD): δ_C 158.6, 131.1, 130.2, 2 × 128.8, 2 × 116.6, 103.8, 32.6, 30.3, 23.4, 14.3.

4.2.1.6. Synthesis of (*E*)-2-methoxy-4-(2-(3-pentylisoxazol-5-yl)vinyl)phenol (76) and (*E*)-4-(2-(3-pentylisoxazol-5-yl)vinyl)phenol (77)

Hydroxylamine hydrochloride (144 mg, 2.1 mmol/134 mg, 1.9 mmol) and pyridine (165 mg = 169 µL, 2.1 mmol/152 mg = 155 µL, 1.9 mmol) were added to a stirred solution of compounds **47** and **71** separately (122 mg, 0.42 mmol/100 mg, 0.38 mmol) in ethanol (4 mL) and refluxed for 6 hrs. The reaction was monitored by TLC. Subsequently, the mixture was cooled to ambient temperature, evaporated in vacuo, and purified by flash chromatography (Silica, gradient elution, 0–20% acetone in *n*-hexane) to afford compound **76**, a pale-yellow solid (96 mg,

79.3%), while product **77** was obtained as a pure compound from the reaction mixture as a pale-yellow solid (98 mg, 99%) [142].

Compound 76. HRESIMS: $C_{17}H_{21}NO_3$, $[M+H]^+$ *m/z* = 288.15999 (calcd 288.15996), ^{1}H NMR (500 MHz, in $CDCl_3$): δ_H 7.22 (d, 1H, *J* = 16.4 Hz), 7.04 (dd, 1H, *J* = 8.1, 2.0 Hz), 7.01 (d, 1H, *J* = 2.0 Hz), 6.92 (d, 1H, *J* = 8.1 Hz), 6.77 (d, 1H, *J* = 16.4 Hz), 6.06 (s, 1H), 5.77 (s, 1H), 3.95 (s, 3H), 2.66 (t, 2H, *J* = 7.5 Hz), 1.68 (m, 2H), 1.37 (m, 2H), 1.36 (m, 2H), 0.91 (t, 3H, *J* = 7.2 Hz) ppm. ^{13}C NMR (125 MHz, in $CDCl_3$): δ_C 168.5, 164.6, 147.0, 134.6, 128.5, 121.5, 114.9, 111.3, 108.9, 100.6, 56.1, 31.5, 28.2, 26.2, 22.5, 14.1.

Compound 77. HRESIMS: $C_{16}H_{19}NO_2$, $[M-H]^-$ *m/z* = 256.13644 (calcd 256.13375). ^{1}H NMR (500 MHz, in $CDCl_3$): δ_H 7.39 (dd, 2H, *J* = 8.6, 1.8 Hz), 7.23 (d, 1H, *J* = 16.4 Hz), 6.85 (dt, 2H, *J* = 8.6, 2.9, 2.1 Hz), 6.77 (d, 1H, *J* = 16.4 Hz), 6.06 (s, 1H), 3.49 (s, 1H), 2.66 (t, 2H, *J* = 7.5 Hz), 1.68 (m, 2H), 1.36 (m, 2H), 1.35 (m, 2H), 0.90 (t, 3H, *J* = 7.2 Hz) ppm. ^{13}C NMR (125 MHz, in $CDCl_3$): δ_C 168.7, 164.6, 157.1, 134.4, 2 × 128.8, 128.6, 2 × 116.0, 111.2, 100.6, 31.5, 28.2, 26.2, 22.5, 14.0.

4.2.1.7. Synthesis of *N*-heptyl-3-(4-hydroxyphenyl) propenamide (81)

A solution of compound **79** (300 mg, 1.5 mmol) in dry CH_2Cl_2 (10 mL) was cooled to 0 °C, DCC (316 mg) and DMAP (18 mg, 0.2 mmol) were added, and the mixture was stirred for 1 h at 0 °C, then heptylamine **80** (153 mg = 0.197 mL) was added and the reaction was monitored over TLC. Subsequently, the solvent was evaporated, redissolved in dichloromethane, washed with $NaHCO_3$ solution, and the organic phase was evaporated to dryness. The product was purified by flash chromatography (Silica, gradient elution of 20-30% acetone in *n*-hexane) to yield compound **81** as a white solid (431 mg, 92.7%) [143].

Compound 81. HRESIMS: $C_{17}H_{27}NO_3$, $[M+H]^+$ *m/z* = 294.20680, (calcd 294.20692), ^{1}H NMR (500 MHz, in $CDCl_3$): δ_H 6.83 (d, 1H, *J* = 8.1 Hz), 6.72 (d, 1H, *J* = 2.0 Hz), 6.68 (dd, 1H, *J* = 8.0, 2.0 Hz), 5.47 (s, 1H), 3.87 (s, 3H), 3.20 (td, 2H, *J* = 7.2, 5.7 Hz), 2.89 (t, 2H, *J* = 7.5 Hz), 2.42 (t, 2H, *J* = 7.5 Hz), 1.43 (m, 2H), 1.26 (m, 8H), 0.88 (t, 3H, *J* = 6.9 Hz) ppm. ^{13}C NMR (125 MHz, in $CDCl_3$): δ_C 172.2, 146.6, 144.2, 133.0, 121.0, 114.5, 111.2, 56.3, 39.7, 39.2, 31.9, 31.7, 29.8, 29.1, 27.0., 22.7, 14.2.

4.2.2. Antiplatelet activity

Antiplatelet activity was studied in collaboration with the group of Prof. Chin-Chung Wu, Graduate Institute of Natural Products, Kaohsiung Medical University, Kaohsiung, Taiwan. Human platelet suspension (3 × 10^8/mL in Tyrode's buffer) was prepared as previously described [144]. The protocol for this study was approved by the institutional review board of Kaohsiung Medical University Hospital (Kaohsiung City, Taiwan). Platelets pre-treated with DMSO (vehicle control) or test compounds were stimulated with AA, and platelet aggregation was measured using turbidimetric aggregometer (Chrono-Log Co., Havertown, PA, USA) at 37 °C under stirring conditions (1200 rpm).

4.2.3. COX-1 inhibitory activity

COX-1 inhibitory activity was tested based on the fluorometric method as described in BioVision's COX-1 inhibitor screening kit leaflet (K548-100, BioVision, CA, USA). Sample solutions were prepared by dissolving in DMSO and subsequently buffer, to get the desired concentrations. In a 96-well white plate (655101, F-bottom, Grenier bio-one, Germany), 80 µL reaction mix (containing 76 µL assay buffer, 1 µL COX Probe, 2 µL COX cofactor, and 1 µL COX-1 enzyme) was added to 10 µL sample solution, DMSO and assay buffer to get test wells assigned for sample screen (S), negative control (N) and blank, respectively. An aliquot of 10 µL of AA/NaOH solution was added to each well using a multichannel pipette to initiate the reaction at the same time, and the fluorescence of each well was measured kinetically at Ex/Em 550/610 nm, at 25 °C for 10 min using a FluoStar Optima plate reader (BMG Labtech, Ortenberg, Germany). The COX inhibitory activity of SC560, a standard inhibitor, was also determined.

The change in fluorescence between two points, T1 and T2 were determined, and relative inhibition was calculated according to the following equation:

$$\% \text{ Inhibition} = (\Delta N - \Delta S)/\Delta N \times 100 \quad (1)$$

where N is the absorbance of the negative control, and S is that of the sample.

Dose-effect studies on the compounds were used to determine the concentration that inhibits 50% of the enzyme activity. The sigmoidal dose–response curves were obtained by using the software GraphPad Prism 8.0 (La Jolla, CA, USA), and these were used to determine the IC_{50} values of the compounds.

4.2.4. Physicochemical character and blood–brain barrier specific permeability

In vitro and *in silico* pharmacokinetic characterization of the compounds was performed in collaboration with Prof. György T. Balogh, Department of Pharmaceutical Chemistry, Semmelweis University, Budapest, Hungary. Basic physicochemical parameters for drug design and candidate selection were calculated by Percepta Software Package (ACD/Labs, Toronto, Ontario, Canada) [145]. Tautomers and their distributions for compounds **47**, **71** and **72** were generated by Marvin Sketch and Tautomer Generator (Chemaxon Ltd., Budapest, Hungary) [146], which is freely accessible with academic license.

For kinetic aqueous solubility studies each sample was dissolved in DMSO to make 10 mM stock solutions. In a 96-well polypropylene plate (Greiner Bio-One, Kremsmünster, Austria), 15 µL stock solutions were added to 285 µL PBS (pH 7.4) to make starting donor solution with 500 µM as target concentration. For each sample, 3 replicates were measured. The samples were covered and shaken at 37 °C, 300 rpm for 2 h (Heidolph Titramax 1000, Heidolph Instruments GmbH & Co. KG, Schwabach, Germany). After that, each sample was transferred into a filter plate (MSSBLPC, Multiscreen Filter plate, Merck kGaA) and filtered (Vacuum Manifold, Merck kGaA, Darmstadt, Germany). The filtrates were transferred into HPLC vials, and acetonitrile (AcN) was added to aliquot to avoid precipitation. The final solvent ratio was AcN:PBS (70:30). Filtrate concentration was determined by HPLC-UV (see Section **4.1**, page 11) using 3-points calibration.

Blood–brain barrier-specific (BBB) permeability measurements were carried out using the PAMPA-BBB model. First, solutions with 500 µM target concentration were prepared as described for the kinetic solubility study. The solutions were sonicated for 10 min at room temperature. To prepare the artificial BBB-specific membrane, 16 mg BPLE were dissolved in 600 µL of *n*-dodecane:*n*-hexane (25:75). Each well of the donor plate (MultiscreenTMIP, MAIPNTR10, pore size 0.45 mm, Merck kGaA) was coated with 5 µL lipid solution and fitted into the acceptor plate containing 300 µL PBS (pH 7.4) with 5% DMSO, and 150–150 µL of the PBS solutions (made from the DMSO stock solutions) were placed on the donor plate's artificial membrane. The sandwich plate system was covered with a tissue of wet paper and a plastic lid to avoid evaporation of the solvent, and it was incubated at 37 ˚C for 4 h. In the end, the initial 500 µM solutions ($c_D(0)$), the donor ($c_D(t)$) and acceptor solution ($c_A(t)$) were analysed by HPLC-UV (see Section **4.1**, page 11). BBB permeability was calculated using the effective permeability equation used for iso-pH conditions described by Avdeef [147] as follows.

$$P_e = \frac{-2.303}{A\cdot(t-\tau_{ss})}\cdot\left(\frac{1}{1+r_v}\right)\cdot \lg\left[-r_v + \#\left(\frac{1+r_v}{1-MR}\right)\cdot\frac{c_D(t)}{c_D(0)}\right] \quad (1)$$

$$MR = 1 - \frac{c_D(t)}{c_D(0)} - \frac{V_A c_A(t)}{V_D c_D(0)} \quad (2)$$

where A is the filter area (0.3 cm^2), V_D and V_A are the volumes in the donor (0.15 cm^3) and acceptor phase (0.3 cm^3), t is the incubation time (s), t_{ss} is the time to reach steady state (s), $c_D(t)$ is the concentration of the compound in the donor phase at time point t (mol/cm^3), $c_D(0)$ is the concentration of the compound in the donor phase at time point zero (mol/cm^3), $c_A(t)$ is the concentration of the compound in the acceptor phase at time point t (mol/cm^3), r_v is the aqueous compartment volume ratio (V_D/V_A).

4.2.5. Antioxidant activity

4.2.5.1. 1,1-Diphenyl-2-picrylhydrazyl (DPPH) scavenging activity

DPPH (1,1-diphenyl-2-picrylhydrazyl) was purchased from Thermo Fisher Scientific. DPPH free radical scavenging assay was performed with some modifications based on the method by Fukomoto et al. [148]. Briefly, in a 96-well microplate, microdilutions of samples (100 µL, starting from 200 µM in HPLC grade MeOH) were made and 100 µL of DPPH reagent (100 µM in MeOH) was added. After 30 min at room temperature in the dark, the absorbance was measured at 550 nm using a FluoStar Optima plate reader (software version 2.20R2, BMG Labtech Ortenberg, Germany). For the blank control, MeOH was used. The scavenging activity was calculated as Inhibition (%) = $(A_0 - A_s)/A_0 \times 100$, and IC_{50} values were calculated by GraphPad Prism 8.0 (La Jolla, CA, USA).

4.2.5.2. Oxygen radical absorbance capacity (ORAC)

AAPH ((2,2'-Azobis(2-methyl-propionamidine) dihydrochloride) and Trolox standard were purchased from Sigma-Aldrich Hungary. Fluorescein was purchased from Fluka Analytical, Tokyo, Japan. ORAC assay was carried out in a 96-well microplate based on the method from

previous study [149]. Briefly, 20 µL of the samples (1 µM final concentration, dissolved in phosphate buffer, pH = 7.4, containing 1% MeOH) were mixed with 60 µL of AAPH (12 mM final concentration, dissolved in phosphate buffer, pH = 7.4) and 120 µL of fluorescein solution (70 nM final concentration, dissolved in phosphate buffer), then the fluorescence was measured (excitation at λ = 485 nm, and emission at λ = 520 nm) through 3 h with 1.5-min cycle intervals with a BMG Labtech FluoStar Optima plate-reader. All experiments were carried out in triplicate, and Trolox was used as standard. The antioxidant capacity is expressed as Trolox Equivalent (TE), as calculated using GraphPad Prism 8.0 (La Jolla, CA, USA).

4.2.5.3. Xanthine oxidase inhibitory activity

The xanthine oxidase (XO) inhibitory activity of the compounds was determined using continuous spectrophotometric rate based on a modified protocol of Sigma. The samples were prepared in a 96-well plate, and the final reaction mixture consisted of 10 µL of sample (dissolved in DMSO, 30 mM stock solution, 100 µM final), 100 µL of xanthine solution (0.15 mM, pH = 7.4), 140 µL of buffer (potassium phosphate, pH = 7.5) and 50 µL of XO (0.2 units/mL). When measuring the enzyme activity, control buffer was used in place of the sample. Allopurinol was applied as a control. The reaction was initiated by the automatic addition of 50 µL of XO solution. The absorbance of XO-induced uric acid production from xanthine was measured at 290 nm for 3 min in a 96-well plate on a BMG Labtech FluoStar Optima plate reader. The inhibitory percentage values were calculated by using Graph Pad Prism 8.0 (La Jolla, CA, USA).

4.2.5.4. Peroxynitrite scavenging activity

Peroxynitrite was synthesised by a continuous flow system using syringe pumps as published previously [150]. Briefly, an acidic solution of hydrogen peroxide (0.6 M H_2O_2, 0.7 M HCl) was pumped to a junction alongside of sodium nitrite solution (0.6 M) at a flow rate of 1.5 mL/min. After passing 10 cm of tubing, it was mixed with a sodium hydroxide solution (1.5 M), also pumped at 1.5 mL/min. The resulting peroxynitrite solution was a bright yellow colour. The tubing around the reaction was submerged in ice. The concentration of the solution was determined by spectrophotometry and was adjusted to 30 mM with 0.1 M NaOH solution.
In a 96-well microplate 245 µL of pyrogallol red (100 µM final concentration, dissolved in 0.1 M glycine buffer) was mixed with 50 µL of sample (0.5 mM final concentration, dissolved in DMSO) and 5 µL $ONOO^-$ solution (500 µM final concentration, freshly prepared). After mixing and keeping it at room temperature for 30 min the absorbance was measured at 550 nm using a FluoStar Optima plate reader (software version 2.20R2, BMG Labtech, Ortenberg, Germany).

4.2.6. Molecular docking

Compounds' structures were drawn and saved in PDB format using ChemDraw 12.0.2 software (ACD/LABS, Advanced Chemistry Development, Inc.). The *h*-COX-1 enzyme structure was retrieved from the PDB database. PDB files for the enzyme and compounds were converted to the PDBQT format using the graphical user interface of AutoDock4 (The Scripps Research Institute) [151]. A grid box (X: -33.050, Y: -47.920, and Z: 0.234; the number of grid points in

the three dimensions [npts]: X: 40, Y: 60, and Z: 60; spacing: 0.375) was set to include the amino acids mentioned by Tóth et al. to characterize the binding site [152]. Docking parameters were set to the default values and ligands were docked via the Lamarckian algorithm. The binding energies were obtained from the resulting DLG files, and interactions visualisation was achieved via Biovia (Discovery Studio visualizer version 21.1.0.20298; Dassault Systèmes, Vélizy-Villacoublay, France) after conversion of the docked PDBQT files into PDB files using OpenBabel GUI software version 2.4.1 [153].

4.3. Thymoquinone-protoflavone hybrids; synthesis, stability, and bioactivity testing

4.3.1. Synthesis

4.3.1.1. Synthesis of 2-isopropyl-5-methylcyclohexa-2,5-diene-1,4-dione (63)

An aliquot of 2g (0.013 mol) of compound **82** was dissolved in 9:1 of AcN: H_2O (50 mL) at room temperature, then (5.7g, 0.013 mol) PIFA was added. The reaction mixture was stirred for 1hr, quenched, and solvents were evaporated under reduced pressure. The resulting mixture was directly purified using flash chromatography (Silica, gradient elution of 0-10% of EtOAc in *n*-hexane) to obtain compound **63** as a yellow crystalline solid (1.11 g, 50.6 %) [76].

4.3.1.2. General procedure for the synthesis of compounds 89–96

The method reported by Z. Szakonyi et al. was used with modifications [143]. Compound **83** or **84** (50 mg, 0.21 mmol/ 30 mg, 0.126 mmol) was dissolved in 2 mL of dry CH_2Cl_2 (5 mL), DMAP was added (2.6 mg, 0.021 mmol/ 1.6 mg, 0.013 mmol) and the mixture was cooled to 0 $^{\circ}$C, then a solution of DCC in dry CH_2Cl_2 was added (44 mg, 0.21 mmol/ 26 mg, 0.126 mmol). The mixture was stirred for 1 h at 0 $^{\circ}$C, after which the corresponding amount (1 eq.) of compounds **62**, **86**, **87**, or **88**, was added and left to stir overnight. The reaction mixture was washed with saturated $NaHCO_3$ solution. The organic layer was collected, dried over Na_2SO_4, filtered and solvent was evaporated under reduced pressure. The resulting mixtures were purified using preparative RP-HPLC (Kinetex, C18, 5µm, 250 x 21.2 mm). Some of them undergo further purification using semipreparative techniques (Agilent, C18, 5 µm, 250 x 10 mm) using wisely selected AcN: H_2O solvent mixtures.

Compound 83: Yellow wax, 12.4%, $C_{13}H_{16}O_4$,HRESIMS: $[M+H]^+$ *m/z* = 237.11199, (calcd 237.11269) ^{1}H NMR (500 MHz, in $CDCl_3$): δ_H = 6.50 (s, 1H), 3.04 (hept, 1H, *J*=6.9 Hz), 2.83 (t, 2H, *J*=7.6 Hz), 2.52 (t, 2H, *J*=7.8 Hz), 2.06 (s, 3H), 1.11 (d, 6H, *J*=6.8 Hz) ppm. ^{13}C NMR (125 MHz, fin $CDCl_3$): δ_C = 188.17, 186.9, 177.5 (only detected on HSQC),154.9, 142.9, 141.5, 130.4, 32.6, 26.9, 22.4, 21.6, 11.9.
Compound 84: Yellow wax, 2.7%, $C_{13}H_{16}O_4$, HRESIMS: $[M+H]^+$ *m/z* = 237.11191, (calcd 237.11269) ^{1}H NMR (500 MHz, in $CDCl_3$): δ_H = 6.48 (s, 1H), 3.06 (hept, 1H, *J*=7.0 Hz), 2.85 (t, 2H, *J*=7.9 Hz), 2.48 (t, 2H, *J*=8.0 Hz), 2.01 (s, 3H), 1.28 (d, 6H, *J*=6.9 Hz) ppm. ^{13}C NMR (125 MHz, in $CDCl_3$): δ_C = 188.1, 187.7, 177.8, 149.9, 144.7, 141.9, 134.6, 33.4, 29.4, 21.6, 21.2, 15.7.

Compound 89: Yellow oil, 12.2 %, $C_{28}H_{24}O_9$, HRESIMS: $[M-H]^-$ *m/z* = 503.13453, (calcd 503.13421) ^{1}H NMR (500 MHz, in $CDCl_3$): δ_H = 12.39 (s, 1H), 6.85 (d, 2H, *J*=9.6 Hz), 6.72 (s, 1H), 6.66 (s, 1H), 6.56 (s, 1H), 6.52 (s, 1H), 6.41 (d, 2H, *J*=9.6 Hz), 3.05 (hept, 1H, *J*=7.0 Hz), 2.92 (t, 2H, *J*=7.7 Hz), 2.73 (t, 2H, *J*=7.7 Hz), 2.09 (s, 3H), 1.12 (d, 6H, *J*=6.8 Hz) ppm. ^{13}C NMR (125 MHz, in $CDCl_3$): δ_C = 188.0, 186.9, 184.4, 182.9, 170.1, 166.4, 162.1, 156.8, 156.2, 154.9, 2 x 145.3, 142.4, 141.7, 2 x 130.6, 130.5, 109.0, 107.9, 106.0, 101.3, 69.7, 33.0, 26.9, 22.4, 21.6, 12.1.

Compound 90: Yellow oil, 8.3 %, $C_{29}H_{26}O_9$, HRESIMS: $[M+H]^+$ *m/z* = 519.16564, (calcd 519.16551) ^{1}H NMR in (500 MHz, in $CDCl_3$): δ_H = 12.43 (s, 1H), 6.75 (d, 2H, *J*=9.7 Hz), 6.70 (s, 1H), 6.63 (s, 1H), 6.58 (s, 1H), 6.56 (s, 1H), 6.53 (d, 2H, *J*=10.9 Hz), 3.41 (s, 3H), 3.05 (hept, 1H, *J*=6.9 Hz), 2.92 (t, 2H, *J*=7.7 Hz), 2.72 (t, 2H, *J*=7.7 Hz), 2.09 (s, 3H), 1.12 (d, 6H, *J*=6.8 Hz) ppm. ^{13}C NMR (125 MHz, in $CDCl_3$): δ_C = 188.0, 186.9, 184.3, 182.9, 170.1, 165.4, 162.1, 156.7, 156.2, 154.9, 2 x 145.1, 142.4, 141.7, 2 x 133.6, 130.5, 109.1, 108.5, 105.9, 101.2, 74.9, 52.9, 33.0, 26.9, 22.4, 21.6, 12.1.

Compound 91: Yellow oil, 8 %, $C_{30}H_{28}O_9$, HRESIMS: $[M+H]^+$ *m/z* = 533.18104, (calcd 533.18116) ^{1}H NMR (500 MHz, in $CDCl_3$): δ_H = 12.44 (s, 1H), 6.79 – 6.74 (m, 3H), 6.62 (s, 1H), 6.56 – 6.51 (m, 4H), 3.58 (q, 2H, *J*=6.9 Hz), 3.05 (hept, 1H, *J*=6.9 Hz), 2.92 (t, 2H, *J*=7.7 Hz), 2.72 (t, 2H, *J*=7.7 Hz), 2.09 (s, 3H), 1.29 (t, 3H, *J*=6.9 Hz), 1.12 (d, 6H, *J*=6.8 Hz) ppm. ^{13}C NMR (125 MHz, in $CDCl_3$): δ_C = 188.0, 186.9, 184.5, 182.9, 170.1, 165.7, 162.1, 156.7, 156.1, 154.9, 2 x 145.6, 142.4, 141.7, 2 x 133.1, 130.5, 109.1, 108.6, 105.9, 101.2, 74.6, 61.1, 33.0, 26.9, 22.4, 21.6, 15.8, 12.1.

Compound 92: Yellow oil, 13.6 %, $C_{32}H_{32}O_9$, MS: $[M+H]^+$ *m/z* = 561.4, (calcd 561.2) ^{1}H NMR (500 MHz, in $CDCl_3$): δ_H = 12.45 (s, 1H), 6.80 – 6.72 (m, 3H), 6.62 (s, 1H), 6.57 – 6.50 (m, 4H), 3.51 (t, 2H, *J*=6.3 Hz), 3.05 (hept, 1H, *J*=7.0 Hz), 2.92 (t, 2H, *J*=7.7 Hz), 2.72 (t, 2H, *J*=7.3 Hz), 2.09 (s, 3H), 1.68 – 1.58 (m, 2H), 1.48 – 1.39 (m, 2H), 1.12 (d, 6H, *J*=6.9 Hz), 0.94 (t, 3H, *J*=7.3 Hz) ppm. ^{13}C NMR (125 MHz, in $CDCl_3$): δ_C = 188.0, 186.9, 184.5, 182.9, 170.1, 165.7, 162.1, 156.7, 156.1, 154.9, 2 x 145.7, 142.4, 141.7, 2 x 133.1, 130.5, 109.1, 108.6, 105.9, 101.2, 74.6, 65.2, 33.0, 32.2, 26.9, 22.4, 21.6, 19.4, 13.9, 12.1.

Compound 93: Yellow oil, 10.9 %, $C_{28}H_{24}O_9$, HRESIMS: $[M+H]^+$ *m/z* = 505.15037, (calcd 505.14986) ^{1}H NMR (500 MHz, in $CDCl_3$): δ_H = 12.37 (s, 1H), 6.86 (d, 2H, *J*=10.1 Hz), 6.72 (s, 1H), 6.67 (d, 1H, *J*=2.0 Hz), 6.58 (d, 1H, *J*=2.0 Hz), 6.50 (d, 1H, *J*=1.6 Hz), 6.41 (d, 2H, *J*=10.0 Hz), 3.08 (hept, 1H, *J*=7.0 Hz), 2.95 (t, 2H, *J*=7.1 Hz), 2.68 (t, 2H, *J*=7.1 Hz), 2.02 (d, 3H, *J*=1.6 Hz), 1.31 (d, 6H, *J*=7.0 Hz) ppm. ^{13}C NMR (125 MHz, in $CDCl_3$): δ_C = 188.2, 187.5, 184.3, 182.9, 169.9, 166.3, 162.1, 156.8, 156.4, 150.1, 2 x 145.2, 144.7, 141.5, 134.7, 2 x 130.7, 109.1, 108.0, 106.1, 101.2, 69.8, 33.9, 29.5, 21.7, 21.3, 15.7.

Compound 94: Yellow oil, 25.8 %, $C_{29}H_{26}O_9$, HRESIMS: $[M+H]^+$ *m/z* = 519.16604, (calcd 519.16551) ^{1}H NMR (500 MHz, in $CDCl_3$): δ_H = 12.41 (s, 1H), 6.75 (d, 2H, *J*=10.3 Hz), 6.70 (s, 1H), 6.64 (d, 1H, *J*=2.1 Hz), 6.58 – 6.54 (m, 3H), 6.50 (d, 1H, *J*=1.6 Hz), 3.41 (s, 3H), 3.08 (hept, 1H, *J*=7.0 Hz), 2.95 (t, 2H, *J*=7.1 Hz), 2.67 (t, 2H, *J*=7.1 Hz), 2.02 (d, 3H, *J*=1.5 Hz), 1.31 (d, 6H, *J*=7.0 Hz) ppm. ^{13}C NMR (125 MHz, in $CDCl_3$): δ_C = 188.1, 187.5, 184.2, 182.9, 169.8, 165.5, 162.1, 156.8, 156.3, 150.1, 2 x 144.9, 144.7, 141.5, 134.7, 2 x 133.6, 109.2, 108.6, 105.9, 101.2, 75.1, 52.9, 33.9, 29.5, 21.7, 21.3, 15.7.

Compound 95: Yellow oil, 13.2%, $C_{30}H_{28}O_9$, HRESIMS: $[M+H]^+$ *m/z* = 533.18172, (calcd 533.18116) ^{1}H NMR (500 MHz, in $CDCl_3$,): δ_H = 12.42 (s, 1H), 6.77 (d, 2H, *J*=10.3 Hz), 6.75 (s, 1H), 6.63 (d, 1H, *J*=2.0 Hz), 6.56 (d, 1H, *J*=2.1 Hz), 6.53 (d, 2H, *J*=10.2 Hz), 6.50 (d, 1H, *J*=1.6 Hz), 3.59 (q, 2H, *J*=7.0 Hz), 3.08 (hept, 1H, *J*=7.0 Hz), 2.95 (t, 2H, *J*=7.1 Hz), 2.67 (t, 2H, *J*=7.1 Hz), 2.02 (d, 3H, *J*=1.6 Hz), 1.32 – 1.2 (m, 9H) ppm. ^{13}C NMR (125 MHz, in $CDCl_3$): δ_C = 188.1, 187.5, 184.4, 182.9, 169.9, 165.7, 162.1, 156.8, 156.2, 150.1, 2 x 145.5, 144.7, 141.5, 134.7, 2 x 133.1, 109.2, 108.6, 105.9, 101.2, 74.7, 61.2, 33.9, 29.4, 21.7, 21.3, 15.8, 15.7.
Compound 96: Yellow oil, 11.3%, $C_{32}H_{32}O_9$, HRESIMS: $[M+H]^+$ *m/z* = 561.21316, (calcd 561.21246) ^{1}H NMR (in $CDCl_3$, 500 MHz): δ_H = 12.45 (s, 1H), 6.77 – 6.73 (m, 3H), 6.63 (d, 1H, *J*=2.0 Hz), 6.56 (d, 1H, *J*=2.1 Hz), 6.53 (d, 2H, *J*=10.1 Hz), 6.50 (d, 1H, *J*=1.6 Hz), 3.52 (t, 2H, *J*=6.3 Hz), 3.07 (hept, 1H, *J*=7.0 Hz), 2.94 (t, 2H, *J*=8.8 Hz), 2.67 (t, 2H, *J*=8.8 Hz), 2.02 (d, 3H, *J*=1.6), 1.67 – 1.59 (m, 2H), 1.48 – 1.39 (m, 2H), 1.31 (d, 6H, *J*=7.0 Hz), 0.95 (t, 3H, *J*=7.4 Hz) ppm. ^{13}C NMR (in $CDCl_3$, 125 MHz): δ_C = 188.1, 187.6, 184.5, 183.0, 169.9, 165.7, 162.1, 156.7, 156.2, 150.1, 2 x 145.7, 144.7, 141.5, 134.6, 2 x 133.1, 109.1, 108.6, 105.9, 101.3, 74.6, 65.2, 33.8, 32.2, 29.5, 21.6, 21.3, 19.4, 15.7, 13.9.

4.3.2. Enzymatic hydrolysis assay

A 0.1 M solution of compound **90** or **94** in AcN was prepared and added to 0.025 M PBS (pH=7.4) equilibrated in a water bath at 37 ˚C. (170 units/ mg protein) Porcine esterase was diluted with 0.025 M PBS then this volume was completed to 2.5 mL with PBS to result in a final compound concentration of 8×10^{-4} M and 1.3 units of enzyme/mL. After 24 hrs. incubation at 37 ˚C, the enzyme activity was quenched and the samples were analyzed via RP- HPLC (Kinetex, C18, 5 µm, 250 x 4.5 mm column, 30-100% AcN gradient elution) [154].

4.3.3. *In vitro* antiproliferative activity

In vitro cell culture-based assays described below were performed in collaboration with Dr. Renáta Minorics and Mr. Bizhar A. Tayeb, Department of Pharmacodynamics and Biopharmacy, Faculty of Pharmacy, University of Szeged, Szeged, Hungary.

4.3.3.1. Cell lines and culture conditions

A collection of gynecological cancer cell lines of human origin including breast cancer like the triple negative MDA-MB-231 and estrogen receptor positive MCF-7, HPV16-positive cervical adenocarcinoma (HeLa) and human glioblastoma (U-87) cell lines were used as *in vitro* models to study the antiproliferative effects of the evaluated compounds. All cell lines were cultivated in T-75 flasks in a minimal essential medium (MEM) supplemented with 10% heat-inactivated fetal bovine serum (FBS), 1% antibiotic-antimycotic mixture (penicillin-streptomycin-amphotericin B) and 1% non-essential amino acids. The cells were incubated at 37 ˚C in a 5% CO_2 incubator. The cells were seeded in 96-well plates at a density of 5 x 10^3 in 100 µL per well, except for the U-87 that were seeded in 1 x 10^4 and incubated at the same conditions for overnight to allow the cells' attachment to the well's bottom before the treatment.

4.3.3.2. Treatment with the compounds

Each of the fifteen prepared compounds was dissolved in dimethyl sulfoxide (DMSO) as a 10 mM standard stock solution and kept at -20 ˚C with minimum light exposure. Immediately before each experiment, the stock solution was used and diluted with a culture medium to get the final concentrations. The values of half-maximal inhibitory concentration (IC_{50}) were determined by exposure of the cells into eight different concentrations of each tested compound (0.39, 0.78, 1.56, 3.125, 6.25, 12.5, 25 and 50 μM). Temozolomide (TMZ) and cisplatin were used as positive controls in the case of U-87 and the gynecological cell lines, respectively. The negative control wells included the cells with only MEM treatment. The plates were incubated for up to 72 hours under the same abovementioned incubation conditions.

4.3.3.3. Antiproliferative activity measurements

The colorimetric MTT assay was used to assess the ability of the prepared compounds to inhibit cellular proliferation. After cells were incubated with the different concentrations of the compounds, 20 μL of the MTT solution ([3-(4,5-dimethylthiazol-2-yl)-2,5-diphenyltetrazolium bromide], 5 mg/mL in PBS, Duchefa Biochemie BV, Haarlem, The Netherlands) was added to each well including the negative controls and kept under the usual incubation conditions for additional four hours. Subsequently, the media was carefully aspirated and 100 μL of DMSO was added to each well and the plates were gently shaken for 30 min to solubilize the precipitated crystals of purple formazan. Absorbance was measured at a wavelength of 545 nm using a microplate UV-VIS reader (SPECTROstar Nano, BMG Labtech GmbH, Offenburg, Germany) [155]. The same procedure was performed using MRC-5 cells to determine the cancer selectivity of the most promising test compounds.

4.3.3.4. Combination Assay

In the case of experimental combination study, cell viability data obtained for equimolar mixtures of the reference fragments were tested in comparison with their corresponding building blocks, as well as with hybrid compounds. The hybrid compounds were regarded as mixtures composed of building fragments in a 1:1 ratio. In this bioassay, at least two separate experiments were performed, each in triplicate. The dataset was then subjected to appropriate statistical analysis. The calculated IC_{50} values were subsequently employed to quantitatively assess the extent of pharmacological benefit obtained through the hybridization of fragments in comparison to the cytotoxic effect produced by the experimental combination of PA or its derivatives and TQ fragments.

4.3.3.5. Statistical analysis

The data from two separate experiments in triplicates were collected to assess the antiproliferative activity of the compounds. The data were calculated and evaluated using the GraphPad Prism 9.5.1 (GraphPad Software, San Diego, CA, USA). The IC_{50} (half-maximal inhibitory concentration) values were determined using log inhibitor vs normalized response of nonlinear regression model of the software. The error bars represent the standard error of mean

(SEM) of the IC_{50} values. The value of the parameter is derived from the ratio of IC_{50} value of test compound on MRC-5 cells and that on U-87 cells. The higher the value, the better the cancer selectivity of the test compound.

5 RESULTS

5.1. 6-Gingerol derivatives

5.1.1. Chemistry

6-G (**1**) was isolated from an ethanolic ginger extract via a feasible extraction process resulting in a pure product with up to 36% yield (**Fig. 5**).

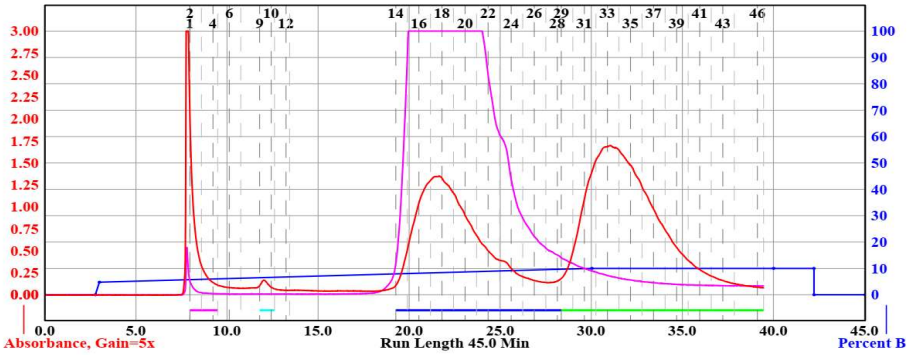

Figure 5. The process of 6-gingerol isolation from the extract via flash chromatography technique using Silica as a stationary phase and n-hexane: acetone as mobile phase (λ_1=225, λ_2=366)

The purified 6-G was subsequently utilized as a starting material for the synthesis of five compounds (**2**, **7**, and **64**–**66**). Except for compound **64**, all of them are naturally present in ginger root. Further derivatives were inspired by the structure of 6-G, and in total fourteen compounds were synthesized (**Schemes 1**, **2**, and **3**); eight of them are new (i.e., compounds **64**, **71**, **73**–**77**, and **81**) according to the SciFinder database.

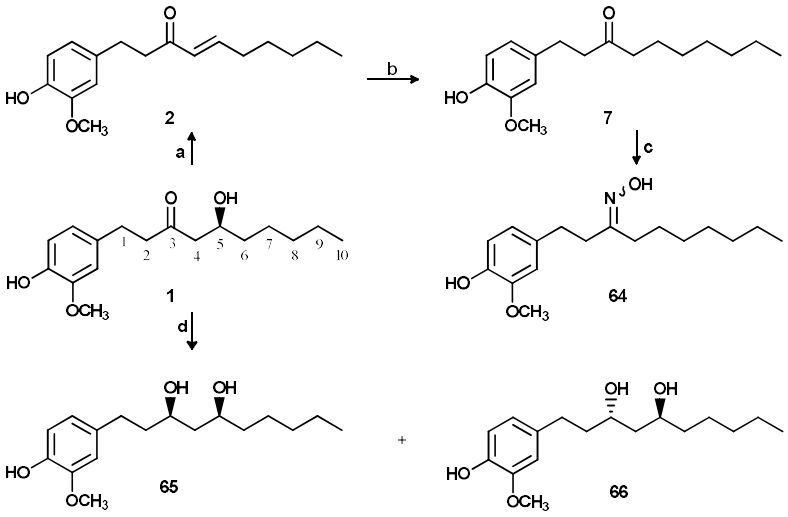

Scheme 1. Semi-synthesis of compounds **2**, **7**, and **64**–**66** from 6-gingerol (**1**). Reaction conditions: **a**. *p*TsOH/toluene/110 ˚C; **b**. H_2/Pd/C/EtOAc/r.t.; **c**. $NH_2OH.HCl$/EtOH/rt; **d**. $NaBH_4$/MeOH.

Compound **2**, 6-shogaol was obtained through a dehydration process using P-TsOH, while 6-gingerdiol epimers, compounds **65** and **66** were gained in a 3:2 ratio mixture product upon 6-G reduction (**Scheme 1**). They were separated using the preparative HPLC technique (**Fig. 6**). Reductive amination of 6-G resulted in compound **64**, an oxime isostere of 6-paradol (compound **7**) and it was obtained as an isomeric mixture of both *E* and *Z* isomer.

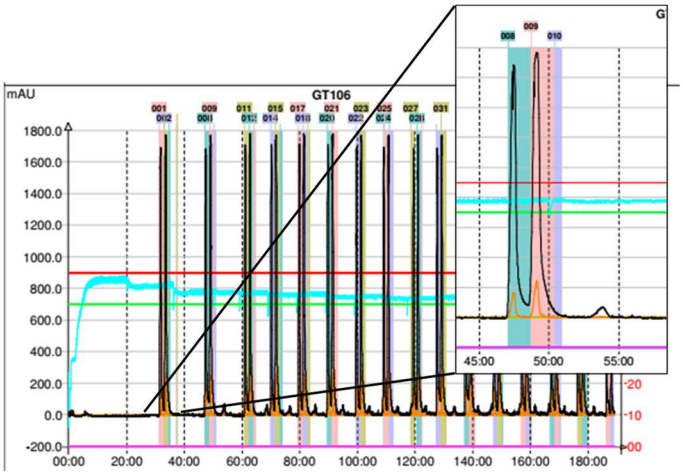

Figure 6. The process of separation of 6-gingerdiol epimers; compounds **65** and **66** using preparative HPLC technique (using Kinetex 5µm XB C-18 250 x 21.2 mm, 50% aqueous AcN).

6-Dehydrogingerdione (**47**) was utilized as a starting material for synthesis of another three products (viz; **72**, **73**, and **76**) (**Scheme 2)**. A similar set of compounds (**74**, **75,** and **77**) was synthesized from compound **71**, a synthetic analogue of **47** prepared similarly to that with the only difference of using 4-hydroxybenzaldehyde **68** instead of vanillin **67**.

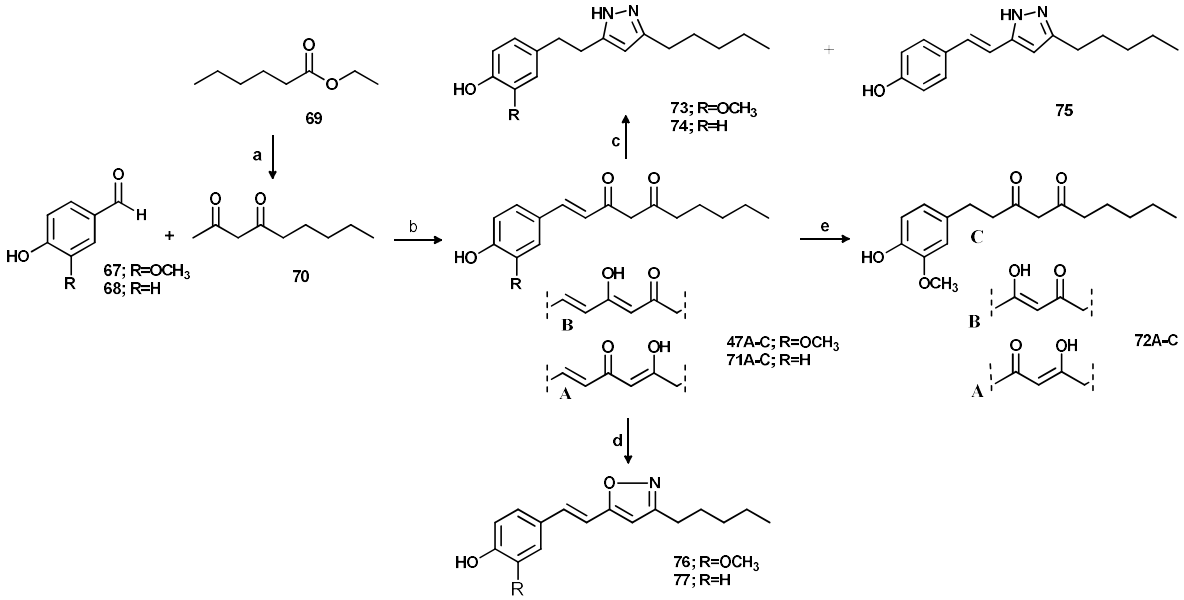

Scheme 2. Preparation of gingerdione derivatives **47, 71** and **72** and their heterocyclic analogues **73**–**77**. Reaction conditions: **a**. 1. NaH/Et_2O/Acetone/0 ˚C, 2. EtOH/HCl; **b**. B_2O_3/ *i*$BuNH_2$/DMF/ 90 ˚C; **c**. H_6N_2O/HCl/EtOH/80 ˚C; **d**. NH_2OH.HCl/pyridine/ethanol/80 ˚C; **e**. H_2/Pd/C/EtOAc /rt. Major tautomers of compounds **47, 71** and **72** are indicated with **A**, **B**, and **C**.

Compound **81** was synthesized as an amide derivative mimicking the structure of 6-G to test the effect of this functional group change in the activity (**Scheme 3**).

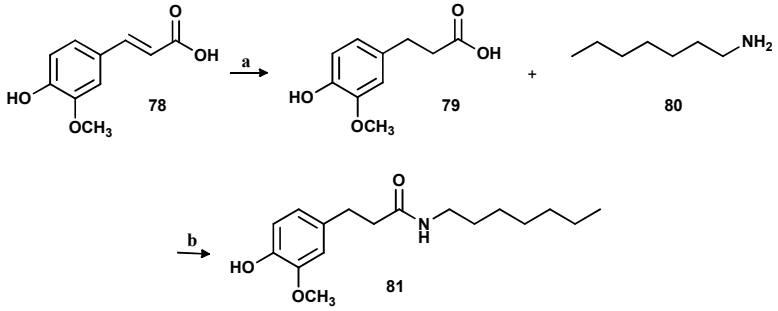

Scheme 3. Preparation of the amide analogue of 6-paradol (**81**). Reaction conditions: **a**. H_2/Pd /C/EtOAc/rt; **b**. DCC/DMAP/CH_2Cl_2/rt.

5.1.2. Antiplatelet activity

The inhibition of AA-induced platelet aggregation was studied using human platelet suspension. Compound **7** proved to be the most potent among all with an IC_{50} of 2.1 μM, while compound **76** was the most promising among the synthetic ones (IC_{50} = 3.1 μM) (**Table 1**). Compounds **65** and **66** were the least active of all.

Table 1. Antiplatelet inhibition assay results. For the assay, washed human platelets were treated with 6-gingerol derivatives for 3 min and then stimulated with arachidonic acid (100 μM); data are presented as mean ± SEM, n = 3; aspirin was used as a positive control.

Compound	Antiplatelet IC_{50} (μM)	$LLE^{a}_{(Antiplatelet)}$
1	45.9 ± 5.1	1.46
2	2.8 ± 0.5	1.40
7	2.1 ± 1.0	1.56
64	5.2 ± 0.4	0.47
65	51.7 ± 2.7	1.26
66	45.1 ± 6.0	1.32
47(A) [b]	4.1 ± 1.0	1.89 [b]
71(A) [b]	71.7 ± 28.3	0.24 [b]
72(B) [b]	3.6 ± 0.9	1.94 [b]
73	4.1 ± 1.2	0.72
74	>100	-
75	3.5 ± 0.9	0.63
76	3.1 ± 0.9	1.08
77	32.0 ± 10.1	−0.27
81	35.9 ± 23.7	0.80
Aspirin	106.0 ± 20.2	2.58

[a] Ligand–lipophilic efficiency: LLE = pIC_{50}—$\log P_{predicted}$. For LLE, green colouring indicates a satisfactory level ($LLE_{(Antiplatelet)} \geq 1.5$ and $IC_{50} \leq 10$ μM). [b] For the sake of strict characterisation, the tautomer with the highest log$P$ value (see **Table 3**) was included in the LLE calculation for compounds **47, 71** and **72**, i.e., the value for the worst possible case is shown in the table.

5.1.3. COX-1 inhibitory activity

Evaluation of the inhibitory activity of the compounds against COX-1 enzyme was conducted using a fluorometric assay. Results are shown below (**Table 2**).

Table 2. Cyclooxygenase-1 (COX-1) inhibition assay results. Data are presented as mean ± SEM, $n = 2$.

Compound	COX-1 IC_{50} (μM)	$LLE^{a}_{(COX-1)}$
1	62.5 ± 23.8	1.30
2	9.8 ± 0.6	0.81
7	4.4 ± 0.2	1.26
64	5.2 ± 0.3	0.48
65	54.3 ± 6.5	1.27
66	76.2 ± 0.3	1.12
47(A) [b]	23.1 ± 9.3	1.14
71(A) [b]	>200	-
72(B) [b]	11.8 ± 5.4	1.53
73	3.6 ± 0.2	0.74
74	>200	-
75	17.5 ± 0.1	−0.04
76	5.85 ± 0.04	0.83
77	>200	-
81	>100	-

[a] Ligand–lipophilic efficiency: LLE = pIC_{50}—$\log P_{predicted}$. For LLE, green colouring indicates a satisfactory level ($LLE_{(COX-1)} \geq 1.0$ and $IC_{50} \leq 10$ μM). [b] For the sake of strict characterisation, the tautomer with the highest log*P* value (see **Table 3**) was included in the LLE calculation for compounds **47, 71** and **72**, i.e., the value for the worst possible case is shown in the table.

5.1.4. Physicochemical character and blood–brain barrier specific permeability

To assess the druggability of these compounds their ADME characteristics were assessed using *in silico* (lead optimisation parameters and the Central Nervous System Multiparameter Optimisation (CNS MPO) compliance [156]) and *in vitro* (determination of kinetic solubility and *in vitro* BBB permeability) approaches. Results along with the calculated descriptors are shown in **Table 3**.

Table 3. *In silico* and experimental data for physicochemical and BBB permeability characterisation. Results are given as mean ± standard error of the mean (SEM); $n = 3$.

		Predicted Values [a]					Experimental Data	
Cmpds ID	Tautomer Distribution (%) [b]	p$K_{a,base}$/ p$K_{a,acid}$ [c]	log$P$/log$D$ $_{pH7.4}$	TPSA	HBD/ HBA	CNS MPO [d] [156]	Kinetic Solubility [e] (μM)	PAMPA-BBB [e'] P_e ($\cdot 10^{-7}$ cm/s)/MR (%)
1		-/10.0	2.9/2.9	66.8	2/4	5.06	>500	35.2 ± 2.4/23.8 ± 1.5
2		-/10.0	4.2/4.2	46.5	1/3	4.18	110.2 ± 3.8	31.7 ± 3.6/20.9 ± 3.9
7		-/10.0	4.1/4.1	46.5	1/3	4.19	45.2 ± 2.7	-/11.0 ± 0.7
64		-/10.1	4.8/4.8	62.1	2/4	3.60	75.1 ± 7.3	-/4.0 ± 11.1
65		-/10.1	3.0/3.0	69.9	3/4	4.72	>500	33.9 ± 2,5/9.1 ± 7.6
66		-/10.1	3.0/3.0	69.9	3/4	4.72	460.7 ± 10.3	27.4 ± 1.6/18.5 ± 2.7
47A	31	-/8.3	**3.5**/3.5	66.8	2/4	4.81		
47B	60	-/8.3	3.2/3.2	66.8	2/4	4.53	54.0 ± 1.3	-/-
47C	9	-/8.7	3.3/3.3	63.6	1/4	5.01		
71A	38	-/8.3	**3.9**/3.8	57.5	2/3	4.62		
71B	54	-/8.4	3.4/3.4	57.5	2/3	4.15	15.6 ± 0.1	-/-
71C	8	-/8.9	3.5/3.5	54.4	1/3	4.75		
72A	31	-/8.7	3.4/3.4	66.8	2/4	4.58	314.6 ± 23.7	
72B	60	-/8.7	**3.5**/3.4	66.8	2/4	4.56		-/-
72C	9	-/9.4	3.3/3.3	63.6	1/4	4.98		
73		3.8/10.1	4.7/4.7	58.1	2/4	3.67	276.7 ± 5.5	15.8 ± 0.8/33.6 ± 4.6
74		3.9/10.1	4.9/4.9	48.9	2/3	3.57	202.9 ± 5.5	20.7 ± 4.3/3.1 ± 5.7
75		3.1/10.0	4.8/4.8	48.9	2/3	3.59	89.4 ± 3.1	-/-
76		-/9.9	4.4/4.4	55.5	1/4	4.04	10.9 ± 2.0	-/-
77		-/9.8	4.8/4.8	46.3	1/3	3.87	<LOD	-/-
81		-/10.1	3.6/3.6	58.6	2/4	4.36	482.6 ± 18.7	32.2 ± 3.4/12.1 ± 5.2
Aspirin		-/3,5	1.4/-1.7	63.6	1/4	5.75	-	-

[a] Predicted values calculated by ACD/Labs Percepta software [145], [b] Generated by Chemaxon Tautomer Generator [146], [c] strongest acidic pK_a, [d] CNS MPO were determined using predicted p$K_{a,basic}$, log$P$/log$D_{pH7.4}$ (classic and consensus settings, respectively), TPSA and HBD values,[e/e'] after 2 h/4 h, at 37 °C in PBS, pH 7.4. *Colours of classification systems*: log$D_{pH7.4}$: moderate violation (yellow) ≥ 3.5, high violation (magenta) ≥ 4.0; CNS MPO: low (magenta) ≤ 4.0, moderate (yellow) ≤ 4.7, good (green) > 4.7; Kin.Sol.: low (magenta) ≤ 100, moderate (yellow) ≤ 300, good (green) > 300; Increased BBB-permeability (green) > 25.

5.1.5. Antioxidant activity

The antioxidant activity was assessed using multiple models, such as the diphenyl-2-picrylhydrazyl (DPPH) scavenging assay, ORAC assay, $ONOO^-$ scavenging, and XO inhibition assays. Compound **65** showed the best activity in the DPPH assay with IC_{50} value of 6.51 μM (**Table 4**).

Table 4. The antioxidant activity results of 6-gingerol and its derivatives. Values are given as mean ± standard error of the mean (SEM). ORAC assay results are given in Trolox equivalents (TE), $ONOO^-$ scavenging and xanthine oxidase (XO) inhibition assay results are given in % inhibition at concentrations of 500 and 100 μM, respectively; $n = 2$ for DPPH; $n = 3$ for ORAC, $ONOO^-$ and XO.

Compounds	DDPH		ORAC TE	$ONOO^-$ Scavenging (%)	XO Inhibition (%)
	IC_{50} (μM)	LLE [a]			
1	8.92 ± 0.46	2.15	1.30 ± 0.04	<5.0	<5.0
2	11.41 ± 0.49	0.75	1.10 ± 0.03	<5.0	<5.0
7	9.43 ± 0.16	0.93	1.36 ± 0.02	<5.0	<5.0
64	8.56 ± 0.07	0.27	0.47 ± 0.09	<5.0	10.56 ± 2.30
65	6.51 ± 0.28	2.19	2.30 ± 0.05	<5.0	<5.0
66	13.82 ± 0.03	1.86	1.12 ± 0.03	<5.0	<5.0
47	9.04 ± 0.19	1.54	1.98 ± 0.12	<5.0	<5.0
71	>200	-	2.89 ± 0.49	<5.0	<5.0
72	10.86 ± 0.69	1.46	2.60 ± 0.06	<5.0	<5.0
73	16.16 ± 0.46	0.09	0.44 ± 0.07	<5.0	10.13 ± 1.65
74	>200	-	1.00 ± 0.02	<5.0	12.30 ± 0.90
75	18.98 ± 1.63	−0.08	2.88 ± 0.16	<5.0	16.01 ± 4.05
76	8.13 ± 0.21	0.69	0.77 ± 0.20	38.40 ± 3.05	<5.0
77	>100	-	1.76 ± 0.06	5.64 ± 1.31	<5.0
81	14.07 ± 0.21	1.25	1.62 ± 0.004	<5.0	<5.0
allopurinol	-	-	-	-	98.80 ± 0.11

[a] Ligand–lipophilic efficiency: LLE = pIC_{50}—$\log P_{predicted}$. For LLE, green colouring indicates a satisfactory level (LLE ≥ 1.5 and IC_{50} ≤ 10 μM).

5.1.6. Molecular docking

To predict the interaction of these compounds with COX-1 enzyme, a molecular docking approach was implemented using AutoDock4.

Compound **76** achieved the best binding affinity (-9.5 Kcal/mol) (for its orientation in the binding pocket, see Discussion, page 35, **Fig. 9**). As compounds **47**, **71**, and **72** are present in both enol and keto forms, their respective enol forms were also docked, and their data are displayed below (**Table 5**).

Table 5. Docking results obtained using AutoDockTools 1.5.7 and Discovery Studio visualizer (21.1.0.20298)

Compound	Binding energy (Kcal/mole)	Number of interacting AA	Number of conventional H-bonds	AA involved in H-bonds
1	-8.68	9	2	Val A:349, Ser A:530
2	-8.76	6	-	-
7	-8.50	9	1	Ile A:523
64	-8.38	11	1	Ser A:530
65	-8.01	11	1	Tyr A:355
66	-7.70	8	2	Val A:349, Ser A:530
47A	-9.29	9	-	-
47B	-8.93	9	1	Tyr A:385
47C	-8.21	4	-	-
71A	-9.23	6	3	Tyr A:385, Gly A:533, ASN A:375
71B	-8.76	5	1	GLY A:533
71C	-8.22	5	1	ASN A:375
72A	-8.30	7	1	Arg A:120
72B	-9.20	9	1	ASN A:375
72C	-8.85	11	-	-
73	-8.88	10	-	-
74	-8.36	9	1	Met A:522
75	-8.47	8	1	Gly A:533
76	-9.50	9	-	-
77	-9.32	12	1	Arg A:376
81	-8.54	10	2	Tyr A:385, Ile A:523

5.2. Protoflavone-thymoquinone hybrids

5.2.1. Chemistry

TQ (**63**) was synthesized from thymol (**82**) using two methods (**Scheme 4**): the first using mCPBA [157], while the second utilizing PIFA as an oxidizing agent [76].

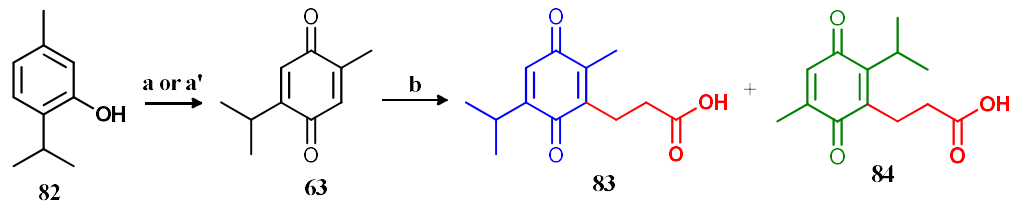

Scheme 4. Preparation of TQ (**63**) and its derivatives; compounds **83** and **84**. Reaction conditions: **a.** mCPBA/$CHCl_3$/rt **a`.** PIFA/AcN: H_2O/rt/1hr **b.**$C_4H_6O_4$/ $AgNO_3$/$(NH_4)_2S_2O_8$/AcN/H_2O/ 100 ˚C

TQ adducts **83** and **84** were then synthesized using succinic acid (**Scheme 4**) and separated via preparative HPLC technique (**Fig. 7.**)

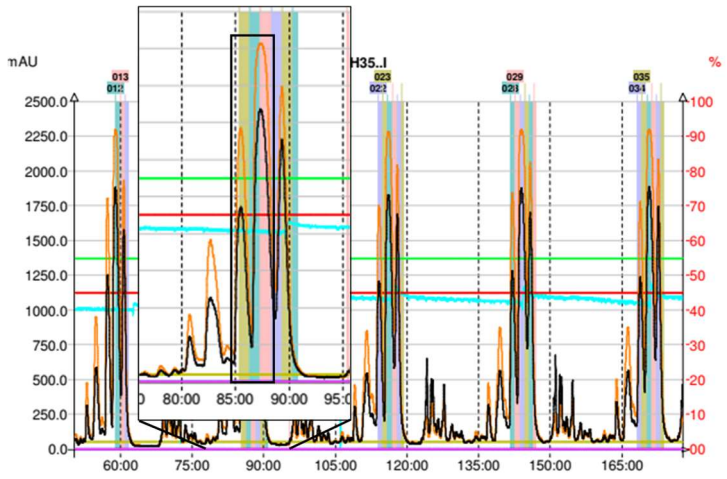

Figure 7: The process of compound **83** and **84** separation using preparative HPLC techniques; (using Kinetex 5µ XB C-18 250 x 21.2 mm, 50% aqueous MeOH).

The protoflavones **62** and **86–88** were synthesized according to the method reported by Hunyadi et al. [76]. Eight hybrid compounds were then synthesized containing different 1'-R groups in the protoflavone B-ring.

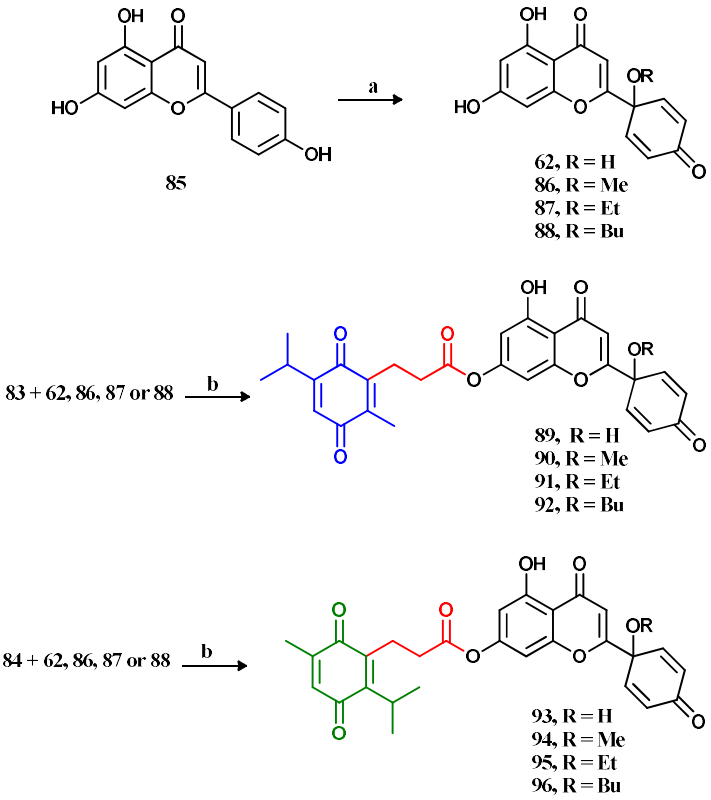

Scheme 5. Preparation of the protoflavone part (**62** and **86–88**) and the corresponding hybrids (**89–96**). Reaction conditions: **a.** PIFA/AcN: ROH/70 ˚C/1hr **b.** DDC/DMAP/dry DCM/rt

The hybrids; compounds **90** and **94** were tested for their stability. Kinetic studies demonstrated a tendency towards hydrolysis by many solvents, especially methanol. The stability for these compounds was also tested in PBS, porcine esterase enzyme, MEM media over time compared to a blank, and a total hydrolysis was noted after 1, 3 and 24 hrs.

5.2.2. *In vitro* antiproliferative activity

The *in vitro* antitumor activity of the hybrid molecules and their building blocks was assessed against HeLa, MCF-7, MDA-MB-123, and U-87 cell lines, results are shown below (**Table 6**)

Table 6. Antiproliferative effects of thymoquinone-protoflavone compounds (hybrids [**90–97**] and their building blocks [**63, 83,** and **84** and **86–89**]) on tested cancer cell lines.

Compounds	Calculated IC_{50} ± SEM; [μM][a]			
	MDA-MB-231	MCF-7	HeLa	U-87
63	7.02 ± 0.17	23.97 ± 1.37	> 100	39.07 ± 3.53
83	38.17 ± 2.81	> 100	> 100	77.72 ± 1.61
84	12.44 ± 0.37	> 100	> 100	88.73 ± 5.17
62	0.57 ± 0.07	0.66 ± 0.06	1.80 ± 0.09	1.73 ± 0.11
86	2.23 ± 0.13	3.95 ± 0.30	5.51 ± 0.21	7.03 ± 0.11
87	1.22 ± 0.03	2.50 ± 0.11	2.83 ± 0.12	1.73 ± 0.06
88	0.82 ± 0.05	2.01 ± 0.07	1.88 ± 0.10	1.50 ± 0.12
89	1.27 ± 0.04	1.65 ± 0.07	2.00 ± 0.26	6.16 ± 0.49
90	2.25 ± 0.13	2.66 ± 0.11	3.51 ± 0.17	7.63 ± 0.46
91	2.15 ± 0.08	3.21 ± 0.07	2.35 ± 0.15	8.22 ± 0.73
92	0.99 ± 0.05	1.68 ± 0.16	1.40 ± 0.25	3.43 ± 0.25
93	0.52 ± 0.02	1.20 ± 0.03	1.06 ± 0.08	1.16 ± 0.20
94	3.53 ± 0.17	5.44 ± 1.32	6.78 ± 0.28	18.89 ± 3.42
95	1.98 ± 0.06	4.11 ± 0.34	1.71 ± 0.16	6.06 ± 0.40
96	1.075 ± 0.08	2.70 ± 0.09	3.08 ± 0.46	8.65 ± 1.15
Cis[b]	9.71 ± 0.51	6.55 ± 0.77	16.01 ± 2.00	9.13 ± 1.79
TMZ[c]	—	—	—	388.2 ± 43.0

[a] Mean value from two independent measurements with three parallel wells

[b] cisplatin

[c] temozolomide

In addition, the experimental combinations (1:1 mixture of building blocks) were tested on the U-87 cells for their antiproliferative activity for the purpose of comparison with the corresponding hybrid compounds (**Table 7**). Generally, a varying degree of potency was noted as evidenced by an IC_{50} range from 1.73 to 11.14 μM across all the experimental combinations.

Table 7. Calculated IC_{50} values of the structural combination (hybrid compounds) and experimental combination of the corresponding thymoquinone and protoflavone building blocks on the U-87 cells. Statistical analysis was performed by using unpaired t-test, * $p<0.05$; *** $p<0.001$ as compared to the corresponding 1:1 fragment mixture.

Compounds		Calculated IC_{50} ± SEM; [μM][a]	
Hybrid	1:1 mixture[b]	Hybrid	1:1 mixture
89	**83 + 62**	6.16 ± 0.49***	2.22 ± 0.43
90	**83 + 86**	7.63 ± 0.46*	10.03 ± 0.87
91	**83 + 87**	8.22 ± 0.73***	3.97 ± 0.23
92	**83 + 88**	3.43 ± 0.25***	1.73 ± 0.08
93	**84 + 62**	1.16 ± 0.20***	3.68 ± 0.35
94	**84 + 86**	18.89 ± 3.42	11.14 ± 1.02
95	**84 + 87**	6.06 ± 0.40	5.82 ± 0.61
96	**84 + 88**	8.65 ± 1.15***	2.90 ± 0.18
-	**63 + 62**	-	3.32 ± 0.54
-	**63 + 86**	-	11.04 ± 0.94
-	**63 + 87**	-	5.89 ± 0.28
	63 + 88	-	0.97 ± 0.42

[a] Mean value from two independent measurements with three parallel wells

[b] Each fragment was administered at the given concentration

Antiproliferative assay on non-cancerous human lung fibroblast cells (MRC-5) to determine their cancer selectivity compared to that of the positive control temozolomide was also conducted using compound **93**, its building blocks (**84** and **62**), their experimental mixture (**84** + **62** in 1:1 ratio), and two additional protoflavone derivatives (**87** and **88**); results shown in table below.

Table 8. Antiproliferative effects of selected compounds on MRC-5 non-cancerous human lung fibroblast cell line and the calculated selectivity indices (SI) of the tested compounds against U-87 glioblastoma cell lines; SI = IC_{50} (MRC-5)/IC_{50} (U-87).

Compound	Calculated IC50 ± SEM; [μM][a] MRC-5	U-87	SI
84	40.25 ± 1.04	88.73 ± 5.17	0.45
62	2.62 ± 0.20	1.73 ± 0.11	1.51
87	3.79 ± 0.25	1.73 ± 0.06	2.19
88	3.56 ± 0.12	1.50 ± 0.12	2.37
93	5.10 ± 0.21	1.16 ± 0.20	4.40
84 + 62 (1:1 mixture)	4.72 ± 0.10	3.68 ± 0.35	1.28
TMZ[b]	1094 ± 45.1	388.2 ± 43.0	2.82

[a] Mean value from two independent measurements with three technical replicates each.

[b] Positive control; TMZ: temozolomide

6. DISCUSSION

6.1. 6-Gingerol derivatives

6.1.1. Chemistry

Structural elucidation for 6-G and its derivatives was performed through HRMS and NMR. In the case of gingerdiones (**47, 71,** and **72**), enol-oxo tautomerization driven by intramolecular hydrogen bond formation resulted in the appearance of signals of both tautomers at different intensities in the spectra. For some of the oxazole or pyrazole derivatives, the peaks for the quaternary carbons in the heterocyclic ring were not identifiable and this might be explained by their long relaxation time after the irradiation. Nevertheless, characteristic ^{1}H proton resonances and HRMS spectra of these compounds allowed the unambiguous establishment of their chemical structures.

Compound **47** was obtained via a total synthetic pathway from vanillin and 2,4-nonanedione according to the method described by Yao et al. [139] (see **Scheme 2**, page 23). The yield of this reaction was very low (11.6%), so different approaches were utilized to improve the yield. A protection-deprotection strategy utilizing different protecting agents didn't really improve the yield (reactions not shown), however, an appreciable increase of *i*-BuNH amount (50% eq. more) and reaction time lead to more than 10% improvement in the yield.

6.1.2. Antiplatelet activity

Platelets represent an important factor in maintaining hemostasis. Imbalances related to them can lead to blood clots resulting in serious conditions like ischemic heart diseases, pulmonary embolism, and stroke. Components of ginger extract were studied for their AA-induced anti-platelet aggregatory activity and encouraging results were reported [30]. The potential antiplatelet activity for isolated 6-G was also reported [46, 158].

One of the pathways that play a crucial role in the process of platelet activation is the arachidonic acid (AA)-cyclooxygenase-1 (COX-1) pathway [159]. To assess the antiplatelet bioactivity of 6-G (**1**) and its derivatives, they were tested for their inhibitory effects on AA-induced platelet aggregation. Except for compound **74**, all compounds showed better platelet-aggregation inhibitory activity compared to the positive control; aspirin (IC_{50} = 106 μM). Compounds **7**, **2**, **76**, **75**, and **72** showed the most promising results, with around 2–4 μM IC_{50} values which is more than 20 folds better than 6-G (**1**) and aspirin (see **Table 1**, page 24). Our results come in accordance with what has been reported previously by Shih et al [62] concerning 6-paradol (**7**) that was the most promising among all.

Regarding the structure-activity relationships, our results suggest an important role for the aromatic methoxy group, which is evident through comparing the IC_{50} values of **47** vs. **71**, **73** vs. **74**, and **76** vs. **77**. Intriguingly, compound **75** didn't follow this rule. This might highlight a possible role of the $\Delta^{1,2}$ olefin in some cases, e.g., when it is conjugated with a pyrazole ring. On the other hand, the 5-OH group substitution is greatly unfavourable; as suggested by the increased antiplatelet activity of compounds **2**, **7**, and **64**, as well as its oxidation (compound **72** vs. **1**) or replacement by a heterocycle (e.g., compound **73** vs. **1**).

Compound **81**, the amide derivative of compound **1** was only moderately active. Comparatively, replacing the 3-oxo group by an oxime group led to only a slight, ca. 2-fold decrease in the antiplatelet activity (IC_{50} = 5.2 µM), which might be explained by different receptor interaction possibilities offered by the hydroxyl group of the oxime functional group.

Ligand-lipophilic efficiency (LLE) is an estimate of drug likeness through linking potency and lipophilicity of a compound, defined as the pIC_{50} of interest minus the LogP of a compound[160, 161]. Notably, most of compounds that showed better results in terms of drug likeness (LLE) are naturally present in ginger root (**72**, **47**, **7**, **1,** and **2**).

6.1.3. COX-1 inhibitory activity:

As cyclooxygenase-1enzyme represents a key factor in the platelet aggregation process, we investigated the activity of our compounds against COX-1 using a fluorometric assay. The antiplatelet mechanism of action of 6-G and its derivatives has previously been suggested to be COX-1 inhibition [46, 63, 162]. Our results for the newly synthesised compounds agree with this notion.

The results are to a great extent in harmony with the antiplatelet inhibition assay results (the IC_{50} datasets of **Table 2** (page 25) give a linear correlation coefficient (R^2) value of 0.887, suggesting the inhibition mechanism to be COX-1-mediated, **Fig. 8**. Compounds **73, 7, 64, 76,** and **2** showed the best IC_{50s}, while compounds **77, 71,** and **74** were the least.

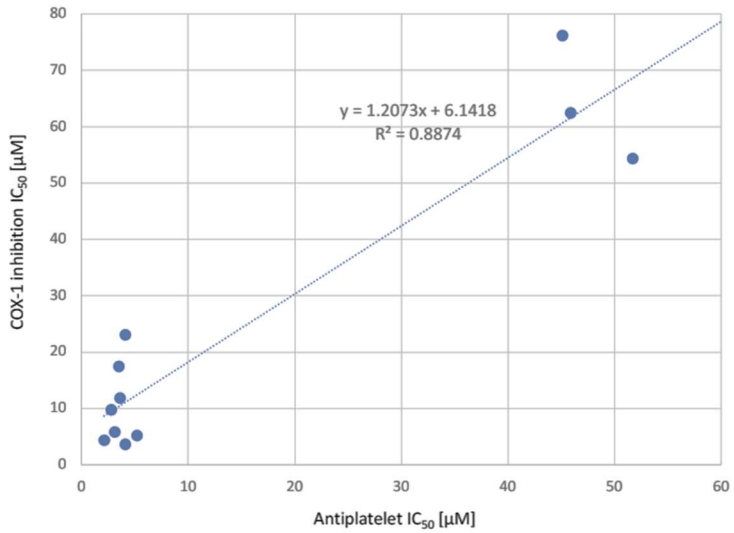

Figure 8: Correlation between the antiplatelet and COX-1 inhibitory activities of the tested compounds. Compounds inactive (IC_{50} > 100 µM on either bioassay, i.e., **71**, **74**, **77**, and **81**) are not included but they fit in the general trend.

6.1.4. Physicochemical Character and Blood–brain Barrier Specific Permeability

To gain a deeper insight into the compounds' drug discovery potential, *in vitro* and *in silico* pharmacokinetic characterization was performed. Above its role in cardiovascular diseases, COX-1 is also a relevant target to the prevention and/or treatment of various neurodegenerative

CNS pathologies with a high inflammatory component (e.g., Alzheimer's disease)[163-165]. Because of this, we expanded our scope to also include CNS specific characterization.

In general, all compounds complied with the components of Lipinski's rule of 5 (Ro5) (molecular weight (250 -300 g/mol), LogP value < 5, less than 10 hydrogen bond acceptors (HBA), and less than 5 hydrogen bond donors (HBD)-results not shown) [166, 167]. Based on this rule and CNS MPO [156] criteria systems, the proton dissociation and lipophilicity properties of 6-G derivatives were compared. The compounds can be classified into three groups according to their acid–base properties: (i) monoprotic phenols (**1**, **2**, **7**, and **64**–**66**, **76**, **77** and **81**), (ii) diprotic amphoterics (imidazole derivatives; **73**–**75**), and (iii) diprotic acids (gingerdione derivatives; **47**, **71**, and **72**). To investigate the distribution of the A-C tautomeric states of derivatives **47**, **71**, and **72**, Chemaxon Ltd.'s freely available Tautomer Generator plugin was used. The results demonstrated that the enol form to be the predominant form (**A**:**B**, ~30:60%), while the dione forms are much less expressed (**C**, ~10**%**). The p*Ka,acid* parameters for these compounds refer to the proton-dissociation behaviour of the enol and dione C-H acid functions in comparison to the aromatic OH function of the other gingerols (**1**, **2**, **7**, and **64**–**66, 73–77**, and **81**).

In term of lipophilicity, though all compounds has logP <5, nevertheless, based on the two-level risk classification created by the lead likeness [168] and CNS MPO criteria (log$D_{pH7.4}$), **2**, **7**, and **64** and **73**–**77** exceed (see **Table 3**, page 26; magenta: high violation), and **81** approach (yellow: moderate violation) the log$D_{pH7.4}$ violation limit. The lipophilicity values of the tautomers of **47**, **71**, and **72** also show a significant difference. The enol forms **A**/**B (47A**, **71A**, **72B)** are more lipophilic than the dione forms (**C**), which was also reflected in their corresponding CNS MPO values. Regarding the polar surface area (TPSA), all the tested gingerols comply with both the Veber's rule (30Å^2 < TPSA < 140Å^2) for bioavailability [169] and the CNS MPO range (40Å^2 < TPSA < 90Å^2) [156]. Based on CNS MPO values; compounds **1**, **2**, **7**, **64**, **65**, **47**, **71**, and **72** (the **C** tautomer form), **76** and **81** (green–yellow) can be classified as suitable candidates for further CNS-targeted preclinical studies. The results also predicted a higher intestinal absorption for compounds **47**, **71**, and **72** compared to the others.

Experimental kinetic solubility (PBS, pH 7.4) and *in vitro* BBB-specific permeability (PAMPA-BBB) of the compounds were also measured. Using a three-level categorization for the kinetic solubility values, compounds **1**, **2**, **65**, **66**, **72**–**74** and **81** were in the acceptable range (greater than 100 μM). PAMPA-BBB study was only applied on these gingerols due to the limitation of poor solubility of other gingerols. Compounds **1**, **2**, **65**, **66** and **81**; marked in green ($P_{e,BBB} \geq 25 \cdot 10\text{-}7$ cm/s) showed increased BBB permeability (see **Table 3**, page 26). Further, compounds **73**–**74** demonstrated adequate BBB penetration characteristics. In contrary, the increased hydrophilic character of compound **72** may compromise its BBB permeability. Despite the relatively high pIC_{50} for compounds **73**, **75,** and **76** in COX-1 inhibition (5.44, 4.76, and 5.23, respectively, not shown in tables), their higher hydrophobicity (LogP > 4.4) compromised their LLE (see **Table 2**, page 25). Accordingly, those compounds showed a relatively high log BB value (1.05, 1.11, and 0.71 respectively) together with compounds **64** and **66** compared to the rest of the compounds (not shown in tables).

6.1.5. Antioxidant activity assay

The antioxidant activity of ginger root extract and its constituents was well reported [170, 171]. Oxidative stress is a hallmark of cardiovascular and neurodegenerative diseases, among many other chronic pathologies [172]. The antioxidant-related cardioprotective effects of 6-G were studied in rats fed with an alcohol/ginger mixed diet. A pronounced suppression of ROS production; restoration of superoxide dismutase and catalase activity, and reduction of alcohol-induced apoptosis in cardiac tissue was noted [58].

We investigated the antioxidant effects of 6-G derivatives in this study using different models. Compound **65** showed the most promising antioxidant activity. Besides its DPPH-scavenging properties, its ORAC value was more than twice as much as that of Trolox. Notably, compound **66**, the 3-epimer of **65**, has only about half of the activity of compound **65** in the DPPH assay and was also weaker in terms of ORAC. Similar to the antiplatelet and COX-1 inhibition assay, the existence of an aromatic methoxy group in the molecule seemed to be important for potent DPPH scavenging activity; except for compound **75**, all compounds without this moiety (**71**, **74**, and **77**) were inactive. In contrary, compounds **71** and **75** were the most promising among all in the ORAC assay, which might point out the complementary value of these two bioassays to evaluate free radical scavenging activity of small molecule antioxidants.

6.1.6. Molecular docking

The *h*-COX-1 enzyme crystal structure was retrieved from the Protein Data Bank (PDB) database (ID: 6Y3C). The binding pocket was identified according to L. Tóth et al. Grid parameters were set to centre at residue Ser530 and to include residues Tyr385, Arg120, and Tyr348 that are in the COX-1 binding pocket [152].They discussed the importance of Tyr385 and Ser530 in the irreversible binding of aspirin to COX-1 active site. Though the new isoxazole-derivative; compound **76**, showed the highest binding affinity (−9.5 Kcal/mol), nevertheless, it did not show any of the above-mentioned interactions with any of these amino acids (**Fig. 9**), however, compound **1**, **64**, and **66** showed hydrogen bonding interactions with Ser530, while compounds **47B**, **71A**, and **81** appeared to interact via hydrogen bonds with Tyr385 (see **Table 5**, page 28).

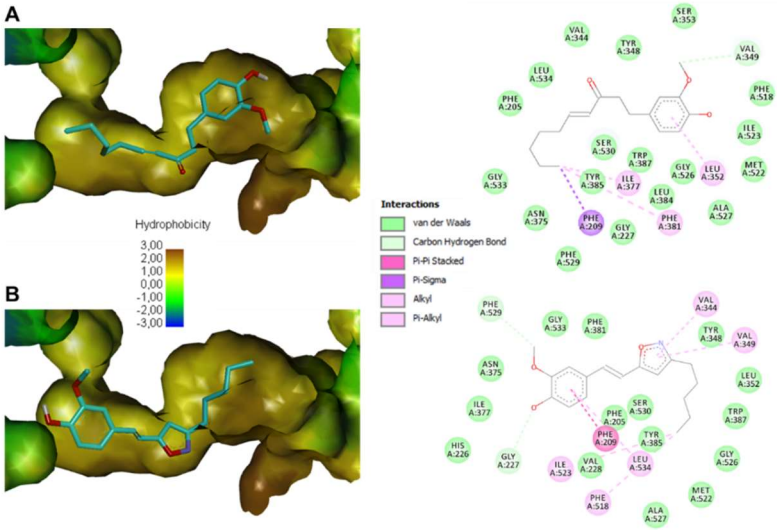

Figure 9. The binding mode of compounds **2** (**A**) and **76** (**B**) on *h*-COX-1 enzyme (PDB ID: 6Y3C) visualised with Discovery studio visualizer (21.1.0.20298); 3D orientation with the enzyme's hydrophobicity surface to the left and 2D representation of the observed interactions to the right. Colour codes for **A** and **B** are identical.

6.2. Protoflavone-thymoquinone hybrids

6.2.1. Chemistry

As TQ (**63**) was synthesized in this work using two different methods, it is worth mentioning that the difference between the two methods was evident in terms of the ease of the purification process and the final yield. The first method was reported by Asakawa et al. using m-CPBA as an oxidizing agent. Though this method was reporting a 47% yield of TQ (**63**), we couldn't achieve that due to the co-elution of TQ and thymol (**82**). Different trials using different solvent systems was not helpful, however, the use of polyamide as a stationary phase and DCM as a mobile phase in a second purification step was to some extent helpful. Nevertheless, the use of multiple purification steps negatively affected the yield (24.2%). The second method using PIFA method resulted in a higher yield from the first purification step (up to 50.6%). To the best of our knowledge, this is the first report for the synthesis of TQ from thymol using PIFA as an oxidizing agent.

TQ was known as a photolabile compound [173] and, to some extent, this character seems to have been also inherited by the hybrids based on our observations on light-exposed samples after 24 h or more (results not shown). Though the synthesis of compounds **83** and **84** has been reported before [136, 174], to our knowledge, this is the first time to report that it results in an isomeric mixture and to successfully isolate the isomers (see **Section 5.2.1**, page 29).

The synthesis of PAG and its derivatives was previously reported [76]. HRMS and 1D and 2D NMR techniques were used for the structural elucidation of all compounds, and spectral data of the known compounds were in good agreement with literature reports. All the protoflavones and the hybrids possess the aromatic region peaks characteristic of the protoflavone B-ring hydrogens with a ^{1}H-^{1}H coupling constant of around 10 Hz. For the TQ derivative compound **83**, the carboxylic quaternary carbon peak could only be detected in the HSQC spectrum.

6.2.2. *In vitro* antiproliferative activity

In general, the protoflavones and the hybrids showed significant activities against the cell lines tested with IC_{50} values lower than 10 μM, except for compound **94** on U-87 cell line, and they demonstrated comparable or stronger activity than the positive controls cisplatin and temozolomide (see **Table 6**, page 30). Most of the antitumor activity of the hybrids could be attributed to the protoflavone fragment as evidenced by the relatively high IC_{50} values obtained for TQ (**63**) and its adducts **83** and **84**. Among the hybrids, compound **93** displayed the most promising results against all cell lines except for MCF-7, with IC_{50} values ranging from 0.51 to 1.20 μM. Though most of the activity of compound **93** could be attributed to its protoflavone fragment, i.e., PA (**62**), it was more selective than that toward the triple-negative breast cancer (TNBC) cell line MDA-MB-231 compared to the hormone-dependent MCF-7 cells with ca.

double activity against the former. This is an important finding in view of the major therapeutic challenges and poor prognosis attributed to TNBC [175]. Interestingly, this selectivity was more evident in terms of TQ with ca. three times higher activity against TNBC, which might suggest that this character of compound **93** was inherited from the TQ fragment (see **Table 6**, page 30). These results may highlight cell-type-specific effects on antiproliferative activity, suggesting further investigation into the underlying mechanisms involved.

Regarding the protoflavone fragments' antitumor activity, PA and its derivatives have been investigated against many cancer cell types including MCF-7 and MDA-MB-231 cell lines. It was noted that a 1'-methoxy substitution of PA compromised the activity, which was, however restored when increasing the length of a non-branching alkyl chain until up to four carbon atoms [76]. Our results come in accordance with this notion for most of the hybrids and for all the protoflavones, however, they deviate at the point of PA (**62**) being more active than the butylated derivative (**88**) against both cell lines. This might be attributed to differences in the experimental conditions and/or variations in the cell lines used by the different research groups. Interestingly, a similar pattern was also observed against HeLa and U-87 cell lines, which may suggest cell line specific limitations for previous findings for protoflavones' SAR.

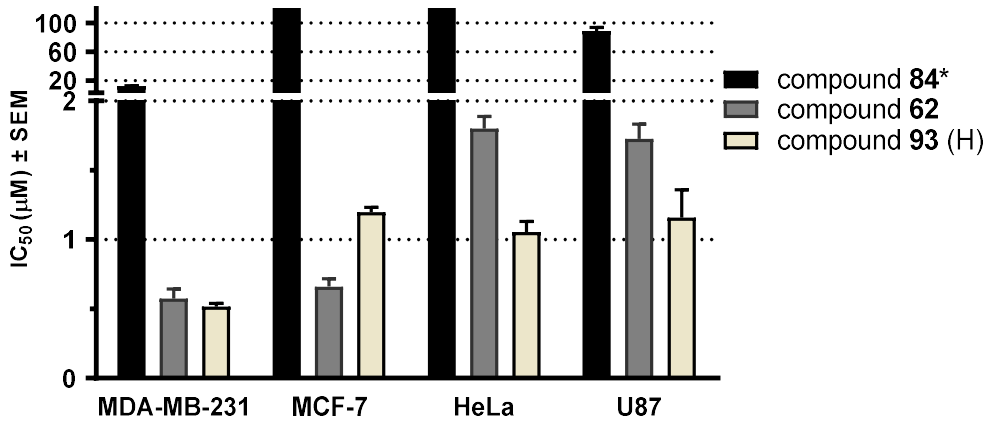

Figure 10. Calculated IC_{50} values of the hybrid (H) compound **93** and its building blocks (compounds **84** and **62**) on the tested cancer cell lines. *Calculated IC_{50} values of compound **84** on MCF-7 and HeLa cells were more than 100 μM.

When comparing the activity of a 1:1 combination of the fragments to their corresponding hybrids against the U-87 cell line, significant differences were observed in several cases (**Fig. 10**).

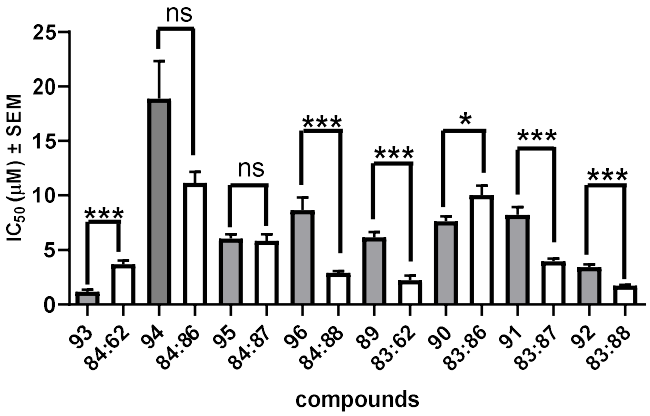

Figure 11. Calculated IC_{50} values of hybrid compounds (■) compared to that of their corresponding experimental combinations (□) determined on U-87 cell line. Statistical analysis was performed by using unpaired t-test.

Intriguingly, the hybrid compounds **93** and **90** exhibited significantly better results (IC_{50} values of 1.16 and 7.63 μM, respectively) compared to the 1:1 combination treatment with their fragments, i.e., compound **83** and **62** (IC_{50}=3.68 μM) or **83** and **86** (IC_{50}=10.03 μM). These results highlight that despite the relatively low chemical stability (see Section **5.2.1**, page 30), these hybrid compounds are much more potent than their fragments combined. Certainly, at this point a reason for this higher potency is not possible to decipher. It may take place due to pharmacodynamic (e.g., the hybrid may bind to different targets) or pharmacokinetic reasons (e.g., more efficient penetration through the cell membrane as hybrid than as separate fragments), or a combination of these. On the other hand, the combination of the fragments; TQ (**63**) and compound **88** showed better activity (0.97 μM) than both the corresponding hybrids (**92** and **96**; 3.4 and 8.7 μM, respectively) and their relative fragments when tested alone (see Table **7**, page 31).

It would be, for instance, of particular interest to evaluate the way compound **93** interferes with p53 and ATR/Chk1 signalling. On one hand, epigenetic reprogramming of p53 by bromodomain-containing protein 8 (BRD8) was most recently discovered as a key to glioblastoma aggressiveness [176]. On the other hand, the inhibition of ATR/Chk1-mediated DNA damage response inhibition is an attractive strategy against glioblastoma [177]. Nevertheless, such studies would require chemically more stable derivatives.

As an initial safety assessment, compound **93**, its building blocks (**84** and **62**), their experimental mixture (**84** + **62** in 1:1 ratio), and two additional protoflavone derivatives (**87** and **88**) were selected for antiproliferative assay on non-cancerous human lung fibroblast cells (MRC-5) to determine their cancer selectivity compared to that of the positive control temozolomide (see **Table 8**; page 31). Selectivity index of compound **84** is lower than 1, which means that it exhibited stronger antiproliferative effect on MRC-5 cells than on U-87 cells. Cancer selectivity of the remaining test compounds has been proven to be higher than 1, i.e., they were more potent against glioblastoma than MRC-5 cells. As an encouraging finding, the hybrid **93** demonstrated the best cancer selectivity (SI=4.40) among the tested compounds, far

exceeding that of the experimental mixture of its building blocks (SI=1.28) and also exceeding that of temozolomide (SI=2.82). For future, related studies, it is also of interest, that the tested protoflavones demonstrated selectivity indices in the same range as that of temozolomide. This result further confirms the potential anti-tumour applications of protoflavones, as well as their pro-drugs.

Altogether compounds **90** and **93** might be regarded as a good starting point for the design of new, promising leads against glioblastoma and/or TNBC. In future, further studies are warranted to overcome the current limitations concerning chemical stability.

7. SUMMARY

The work presented in this thesis can be briefly summarized as follows.

6-Gingerol derivatives: Fifteen compounds have been synthesized, eight of them are new (**64**, **71**, **73**—**77**, **81**), while the rest are naturally present in ginger root (**1**, **2**, **7**, **47**, **65, 66**, and **72**). Chemical changes were introduced into the structure of 6-gingerol (the functional groups of the aliphatic side chain and/or the aromatic methoxy group) through different synthetic strategies, and various chromatographic techniques were used to purify the products. The potential cardiovascular protective and antioxidant effects of the compounds were tested by *in vitro* bioassays combined with *in silico* and *in vitro* pharmacokinetic analysis and *in silico* molecular docking study. Compounds **7**, **2**, **76**, **75**, and **72** showed the most promising antiplatelet activity among all. A linear correlation coefficient (R^2) value of 0.887 for the COX-1 inhibitory activity results suggested this pathway to be responsible for the antiplatelet action. Considering the results of the pharmacokinetic analysis and molecular docking of those compounds, compound **2** may be pointed out as the most promising lead worthy for further preclinical studies, while compounds **7**, **47** and the new semisynthetic compound **76** are hits that require further structural optimization to improve their aqueous solubility. Concerning the antioxidant activity, Compounds **65**, **76**, **64**, **1**, and **47** were the most active in the diphenyl-2-picrylhydrazyl (DPPH) scavenging capacity assay, while compounds **71** and **75** showed the best activity in the ORAC TE assay.

Thymoquinone-protoflavone hybrids: Eight new ester-linked hybrid compounds (**89**—**96**) have been synthesized and tested for their antiproliferative activity, along with their corresponding fragments **25**, **62**, **83**, **84**, and **86**—**88** (alone and in combination) against four human cancer cell lines viz. HeLa, MCF-7, MDA-MB-231 and U-87. TQ and the protoflavones were semi-synthesized from their naturally occurring thymol and apigenin, respectively. After introducing a linker moiety into TQ, the adducts were coupled to different protoflavones through DCC-catalyzed esterification. The chemical stability of the hybrids was unfortunately rather poor in cell culture medium, showing complete hydrolysis in MEM after one hour upon incubation at 37 °C. Despite this character, some encouraging antitumor properties were revealed. The bioactivity of the hybrid molecules was mostly attributed to the protoflavones part (**62**, **86**—**88**), as TQ and it is adducts showed much weaker activity. Still, the hybrid compound **93** showed the best activity (ranging from 0.51—1.2 μM) among all hybrids and protoflavones against all cell lines except for MCF-7. Compound **93** also showed the highest selectivity against the TNBC cell line MDA-MB-231 compared to MCF-7, and the highest tumor selectivity against U-87 glioblastoma vs. MRC-5 fibroblasts. Despite their relatively low chemical stability, the hybrid compounds **90** and **93** acted significantly stronger against U-87 cells than the 1:1 combination of their corresponding fragments. This encourages further studies into such hybrid molecules, which, after a necessary improvement of their chemical stability, may provide valuable new antitumor agents.

REFERENCES

1. WHO. *Cancer*. 2022; Available from: https://www.who.int/health-topics/cancer#tab=tab_1
2. WHO. *Cardiovascular diseases*. 2022; Available from: https://www.who.int/health-topics/cardiovascular-diseases#tab=tab_1.
3. WHO. *Cardiovascular diseases*. 2021; Available from: https://www.who.int/health-topics/cardiovascular-diseases#tab=tab_1.
4. Newman, D.J., *Natural products and drug discovery.* Natl Sci Rev, 2022. **9**(11): nwac206.
5. Newman, D.J. and G.M. Cragg, *Natural Products as Sources of New Drugs over the Nearly Four Decades from 01/1981 to 09/2019.* J Nat Prod, 2020. **83**(3): p. 770-803.
6. Wang, C., A. Aguilar, and I. Ojima, *Strategies for the drug discovery and development of taxane anticancer therapeutics.* Expert Opin Drug Discov, 2022. **17**(11): p. 1193-1207.
7. Ahmad Dar, A., P.L. Sangwan, and A. Kumar, *Chromatography: An important tool for drug discovery.* J Sep Sci, 2020. **43**(1): p. 105-119.
8. Varela, M.T. and J.P.S. Fernandes, *Natural Products: Key Prototypes to Drug Discovery Against Neglected Diseases Caused by Trypanosomatids.* Curr Med Chem, 2020. **27**(13): p. 2133-2146.
9. Barnes, E.C., R. Kumar, and R.A. Davis, *The use of isolated natural products as scaffolds for the generation of chemically diverse screening libraries for drug discovery.* Nat Prod Rep, 2016. **33**(3): p. 372-81.
10. Liao, J., et al., *In Silico Methods for Identification of Potential Active Sites of Therapeutic Targets.* Molecules, 2022. **27**(20): p. 7103.
11. Frusciante, L., et al., *Artificial Intelligence Approaches in Drug Discovery: Towards the Laboratory of the Future.* Curr Top Med Chem, 2022. **22**(26): p. 2176-2189.
12. Maghsoudi, S., et al., *A review on computer-aided chemogenomics and drug repositioning for rational COVID-19 drug discovery.* Chem Biol Drug Des, 2022. **100**(5): p. 699-721.
13. Vemula, D., et al., *CADD, AI and ML in Drug Discovery: A Comprehensive Review.* Eur J Pharm Sci, 2023. **181**: p. 106324.
14. Yahyazadeh, R., et al., *Promising effects of gingerol against toxins: A review article.* Biofactors, 2021. **47**(6): p. 885-913.
15. Fakhri, S., et al., *Ginger and Heart Health: From Mechanisms to Therapeutics.* Curr Mol Pharmacol, 2020. **14**(6): p. 943-959.
16. Roudsari, N.M., et al., *Ginger: A complementary approach for management of cardiovascular diseases.* Biofactors, 2021. **47**(6): p. 933-951
17. Gawel, K., et al., *6-Gingerol, a Major Constituent of Zingiber officinale Rhizoma, Exerts Anticonvulsant Activity in the Pentylenetetrazole-Induced Seizure Model in Larval Zebrafish.* Int J Mol Sci, 2021. **22**(14): p. 7745.
18. Shukla, Y. and M. Singh, *Cancer preventive properties of ginger: a brief review.* Food Chem Toxicol, 2007. **45**(5): p. 683-90.
19. Dalsasso, R.R., G.A. Valencia, and A.R. Monteiro, *Impact of drying and extractions processes on the recovery of gingerols and shogaols, the main bioactive compounds of ginger.* Food Res Int, 2022. **154**: p. 111043.
20. Mao, Q.Q., et al., *Bioactive Compounds and Bioactivities of Ginger (Zingiber officinale Roscoe).* Foods, 2019. **8**(6): p. 185.
21. Saxena, R., et al., *Ginger augmented chemotherapy: A novel multitarget nontoxic approach for cancer management.* Mol Nutr Food Res, 2016. **60**(6): p. 1364-73.
22. Sp, N., et al., *Potential Antitumor Effects of 6-Gingerol in p53-Dependent Mitochondrial Apoptosis and Inhibition of Tumor Sphere Formation in Breast Cancer Cells.* Int J Mol Sci, 2021. **22**(9): p. 4660.
23. Hughes, T., S. Azim, and Z. Ahmad, *Inhibition of Escherichia coli ATP synthase by dietary ginger phenolics.* Int J Biol Macromol, 2021. **182**: p. 2130-2143.

24. Hayati, R.F., et al., *[6]-Gingerol Inhibits Chikungunya Virus Infection by Suppressing Viral Replication.* Biomed Res Int, 2021. **2021**: p. 6623400.
25. Abolaji, A.O., et al., *Protective properties of 6-gingerol-rich fraction from Zingiber officinale (Ginger) on chlorpyrifos-induced oxidative damage and inflammation in the brain, ovary and uterus of rats.* Chem Biol Interact, 2017. **270**: p. 15-23.
26. Dugasani, S., et al., *Comparative antioxidant and anti-inflammatory effects of [6]-gingerol, [8]-gingerol, [10]-gingerol and [6]-shogaol.* J Ethnopharmacol, 2010. **127**(2): p. 515-20.
27. Almatroodi, S.A., et al., *6-Gingerol, a Bioactive Compound of Ginger Attenuates Renal Damage in Streptozotocin-Induced Diabetic Rats by Regulating the Oxidative Stress and Inflammation.* Pharmaceutics, 2021. **13**(3): p. 317.
28. Liu, L., et al., *6-Gingerol Improves Ectopic Lipid Accumulation, Mitochondrial Dysfunction, and Insulin Resistance in Skeletal Muscle of Ageing Rats: Dual Stimulation of the AMPK/PGC-1α Signaling Pathway via Plasma Adiponectin and Muscular AdipoR1.* Mol Nutr Food Res, 2019. **63**(6): p. e1800649.
29. Guo, X.X., et al., *Ginger and 6-gingerol prevent lipopolysaccharide-induced intestinal barrier damage and liver injury in mice.* J Sci Food Agric, 2022. **102**(3): p. 1066-1075.
30. Liao, Y.R., et al., *Anti-platelet aggregation and vasorelaxing effects of the constituents of the rhizomes of Zingiber officinale.* Molecules, 2012. **17**(8): p. 8928-37.
31. Hibino, T., et al., *Goshuyuto, a traditional Japanese medicine for migraine, inhibits platelet aggregation in guinea-pig whole blood.* J Pharmacol Sci, 2008. **108**(1): p. 89-94.
32. Adetuyi, B.O. and E.O. Farombi, *6-Gingerol, an active constituent of ginger, attenuates lipopolysaccharide-induced oxidation, inflammation, cognitive deficits, neuroplasticity, and amyloidogenesis in rat.* J Food Biochem, 2021. **45**(4): p. e13660.
33. Poltronieri, J., et al., *[6]-gingerol as a cancer chemopreventive agent: a review of its activity on different steps of the metastatic process.* Mini Rev Med Chem, 2014. **14**(4): p. 313-21.
34. Chrubasik, S., M.H. Pittler, and B.D. Roufogalis, *Zingiberis rhizoma: a comprehensive review on the ginger effect and efficacy profiles.* Phytomedicine, 2005. **12**(9): p. 684-701.
35. McEwen, B.J., *The influence of diet and nutrients on platelet function.* Semin Thromb Hemost, 2014. **40**(2): p. 214-26.
36. Abebe, W., *Herbal medication: potential for adverse interactions with analgesic drugs.* J Clin Pharm Ther, 2002. **27**(6): p. 391-401.
37. Mousa, S.A., *Antithrombotic effects of naturally derived products on coagulation and platelet function.* Methods Mol Biol, 2010. **663**: p. 229-40.
38. Chen, C., et al., *In vitro anti-platelet aggregation effects of fourteen fruits and vegetables.* Pak J Pharm Sci, 2019. **32**(1): p. 185-195.
39. Khodadi, E., *Platelet Function in Cardiovascular Disease: Activation of Molecules and Activation by Molecules.* Cardiovasc Toxicol, 2020. **20**(1): p. 1-10.
40. Srivas, K.C., *Effects of aqueous extracts of onion, garlic and ginger on platelet aggregation and metabolism of arachidonic acid in the blood vascular system: in vitro study.* Prostaglandins Leukot Med, 1984. **13**(2): p. 227-35.
41. Jiang, X., et al., *Effect of ginkgo and ginger on the pharmacokinetics and pharmacodynamics of warfarin in healthy subjects.* Br J C Pharmacol, 2005. **59**(4): p. 425-432.
42. Lumb, A.B., *Effect of dried ginger on human platelet function.* Thromb Haemost, 1994. **71**(1): p. 110-1.
43. Young, H.Y., et al., *Synergistic effect of ginger and nifedipine on human platelet aggregation: a study in hypertensive patients and normal volunteers.* Am J Chin Med, 2006. **34**(4): p. 545-51.
44. Lv, X.-W., et al., *6-Gingerol relieves myocardial ischaemia/reperfusion injury by regulating lncRNA H19/miR-143/ATG7 signaling axis-mediated autophagy.* Lab Invest, 2021. **101**(7): p. 865-877.

45. Wang, S., et al., *6-Gingerol Ameliorates Behavioral Changes and Atherosclerotic Lesions in ApoE(-/-) Mice Exposed to Chronic Mild Stress.* Cardiovasc Toxicol, 2018. **18**(5): p. 420-430.
46. Guh, J.H., et al., *Antiplatelet effect of gingerol isolated from Zingiber officinale.* J Pharm Pharmacol, 1995. **47**(4): p. 329-32.
47. Lv, X., et al., *6-Gingerol Activates PI3K/Akt and Inhibits Apoptosis to Attenuate Myocardial Ischemia/Reperfusion Injury.* Evid Based Complement Alternat Med, 2018. **2018**: p. 9024034.
48. Ornelas, A., et al., *Beyond COX-1: the effects of aspirin on platelet biology and potential mechanisms of chemoprevention.* Cancer metastasis rev, 2017. **36**(2): p. 289-303.
49. Rucker D, D.A., *Thromboxane A2*, in *Physiology*. 2021, StatPearls. Publishing; Available from: https://www.ncbi.nlm.nih.gov/books/NBK539817/
50. Miciaccia, M., et al., *Three-dimensional structure of human cyclooxygenase (hCOX)-1.* Sci Rep, 2021. **11**(1): p. 4312.
51. Picot, D., P.J. Loll, and R.M. Garavito, *The X-ray crystal structure of the membrane protein prostaglandin H2 synthase-1.* Nature, 1994. **367**(6460): p. 243-9.
52. Xu, S., et al., *Oxicams bind in a novel mode to the cyclooxygenase active site via a two-water-mediated H-bonding Network.* J Biol Chem, 2014. **289**(10): p. 6799-6808.
53. Blobaum, A.L. and L.J. Marnett, *Structural and Functional Basis of Cyclooxygenase Inhibition.* J Med Chem, 2007. **50**(7): p. 1425-1441.
54. Marnett, L.J., et al., *Arachidonic acid oxygenation by COX-1 and COX-2. Mechanisms of catalysis and inhibition.* J Biol Chem, 1999. **274**(33): p. 22903-6.
55. Nugteren, D.H. and E. Hazelhof, *Isolation and properties of intermediates in prostaglandin biosynthesis.* Biochim Biophys Acta, 1973. **326**(3): p. 448-61.
56. Mohd Sahardi, N.F.N. and S. Makpol, *Ginger (Zingiber officinale Roscoe) in the Prevention of Ageing and Degenerative Diseases: Review of Current Evidence.* Evid Based Complement Alternat Med, 2019. **2019**: p. 5054395.
57. Ivane, N.M.A., et al., *The anti-oxidative potential of ginger extract and its constituent on meat protein isolate under induced Fenton oxidation.* J Proteomics, 2022. **269**: p. 104723.
58. Ganjikunta, V.S., et al., *Cardioprotective Effects of 6-Gingerol against Alcohol-Induced ROS-Mediated Tissue Injury and Apoptosis in Rats.* Molecules, 2022. **27**(23).
59. Han, X., et al., *6-Gingerol exerts a protective effect against hypoxic injury through the p38/Nrf2/HO-1 and p38/NF-κB pathway in H9c2 cells.* J Nutr Biochem, 2022. **104**: p. 108975.
60. Manjunathan, T., et al., *6-Gingerol and Semisynthetic 6-Gingerdione Counteract Oxidative Stress Induced by ROS in Zebrafish.* Chem Biodivers, 2021. **18**(12): p. e2100650.
61. Ahmed, S.H.H., T. Gonda, and A. Hunyadi, *Medicinal chemistry inspired by ginger: exploring the chemical space around 6-gingerol.* RSC Adv, 2021. **11**(43): p. 26687-26699.
62. Shih, H.C., et al., *Synthesis of analogues of gingerol and shogaol, the active pungent principles from the rhizomes of Zingiber officinale and evaluation of their anti-platelet aggregation effects.* Int J Mol Sci, 2014. **15**(3): p. 3926-51.
63. Koo, K.L., et al., *Gingerols and related analogues inhibit arachidonic acid-induced human platelet serotonin release and aggregation.* Thromb Res, 2001. **103**(5): p. 387-97.
64. Giaquinto, A.N., et al., *Breast Cancer Statistics, 2022.* CA Cancer J Clin, 2022. **72**(6): p. 524-541.
65. WCRF. *Worldwide cancer data*. 2020 ; Available from: www.wcrf.org/cancer-trends/worldwide-cancer-data/.
66. Davis, M.E., *Glioblastoma: Overview of Disease and Treatment.* Clin J Oncol Nurs, 2016. **20**(5 Suppl): p. S2-8.
67. Aiello, P., et al., *Medicinal Plants in the Prevention and Treatment of Colon Cancer.* Oxid Med Cell Longev, 2019. **2019**: p. 2075614.
68. Buyel, J.F., *Plants as sources of natural and recombinant anti-cancer agents.* Biotechnol Adv, 2018. **36**(2): p. 506-520.

69. Garima, S., et al., *Ethnobotanical survey of medicinal plants used in the management of cancer and diabetes.* J Tradit Chin Med, 2020. **40**(6): p. 1007-1017.
70. Zhou, Y., et al., *Natural Polyphenols for Prevention and Treatment of Cancer.* Nutrients, 2016. **8**(8): p. 515.
71. Benarba, B. and A. Pandiella, *Colorectal cancer and medicinal plants: Principle findings from recent studies.* Biomed Pharmacother, 2018. **107**: p. 408-423.
72. Khan, T., et al., *Anticancer Plants: A Review of the Active Phytochemicals, Applications in Animal Models, and Regulatory Aspects.* Biomolecules, 2019. **10**(1): p. 47.
73. Lin, A.S., et al., *New cytotoxic flavonoids from Thelypteris torresiana.* Planta Med, 2005. **71**(9): p. 867-70.
74. Lin, A.S., et al., *Novel flavonoids of Thelypteris torresiana.* Chem Pharm Bull, 2007. **55**(4): p. 635-7.
75. Yuan, Q., et al., *A novel, broad-spectrum antitumor compound containing the 1-hydroxycyclohexa-2,5-dien-4-one group: The disclosure of a new antitumor pharmacophore in protoapigenone 1.* Bioorganic Med Chem Let, 2011. **21**(11): p. 3427-3430.
76. Hunyadi, A., et al., *Direct semi-synthesis of the anticancer lead-drug protoapigenone from apigenin, and synthesis of further new cytotoxic protoflavone derivatives.* PLoS One, 2011. **6**(8): p. e23922.
77. Chang, H.L., et al., *Protoapigenone, a novel flavonoid, inhibits ovarian cancer cell growth in vitro and in vivo.* Cancer Lett, 2008. **267**(1): p. 85-95.
78. Chen, W.Y., et al., *Protoapigenone, a natural derivative of apigenin, induces mitogen-activated protein kinase-dependent apoptosis in human breast cancer cells associated with induction of oxidative stress and inhibition of glutathione S-transferase π.* Invest New Drugs, 2011. **29**(6): p. 1347-59.
79. Chen, Y.J., et al., *Total synthetic protoapigenone WYC02 inhibits cervical cancer cell proliferation and tumour growth through PIK3 signalling pathway.* Basic Clin Pharmacol Toxicol, 2013. **113**(1): p. 8-18.
80. Chiu, C.C., et al., *Fern plant-derived protoapigenone leads to DNA damage, apoptosis, and G(2)/m arrest in lung cancer cell line H1299.* DNA Cell Biol, 2009. **28**(10): p. 501-6.
81. Csekes, E., et al., *Protoflavones in melanoma therapy: Prooxidant and pro-senescence effect of protoapigenone and its synthetic alkyl derivative in A375 cells.* Life Sci, 2020. **260**: p. 118419.
82. Dankó, B., et al., *Synthesis and SAR Study of Anticancer Protoflavone Derivatives: Investigation of Cytotoxicity and Interaction with ABCB1 and ABCG2 Multidrug Efflux Transporters.* ChemMedChem, 2017. **12**(11): p. 850-859.
83. Wang, H.C., et al., *Inhibition of ATR-dependent signaling by protoapigenone and its derivative sensitizes cancer cells to interstrand cross-link-generating agents in vitro and in vivo.* Mol Cancer Ther, 2012. **11**(7): p. 1443-53.
84. Chang, H.L., et al., *Protoapigenone, a novel flavonoid, induces apoptosis in human prostate cancer cells through activation of p38 mitogen-activated protein kinase and c-Jun NH2-terminal kinase 1/2.* J Pharmacol Exp Ther, 2008. **325**(3): p. 841-9.
85. Lin, A.-S., et al., *First total synthesis of protoapigenone and its analogues as potent cytotoxic agents.* J Med Chem, 2007. **50**(16): p. 3921-3927.
86. Chen, H.M., et al., *A novel synthetic protoapigenone analogue, WYC02-9, induces DNA damage and apoptosis in DU145 prostate cancer cells through generation of reactive oxygen species.* Free Radic Biol Med, 2011. **50**(9): p. 1151-62.
87. Yeh, B.W., et al., *The protoapigenone analog WYC0209 targets CD133+ cells: A potential adjuvant agent against cancer stem cells in urothelial cancer therapy.* Toxicol Appl Pharmacol, 2020. **402**: p. 115129.
88. Chen, Y.J., et al., *The synthetic flavonoid WYC02-9 inhibits colorectal cancer cell growth through ROS-mediated activation of MAPK14 pathway.* Life Sci, 2013. **92**(22): p. 1081-92.

89. Yuan, Q., et al., *A novel, broad-spectrum antitumor compound containing the 1-hydroxycyclohexa-2,5-dien-4-one group: the disclosure of a new antitumor pharmacophore in protoapigenone 1.* Bioorg Med Chem Lett, 2011. **21**(11): p. 3427-30.
90. Xue, P., et al., *A novel compound RY10-4 downregulates P-glycoprotein expression and reverses multidrug-resistant phenotype in human breast cancer MCF-7/ADR cells.* Biomed Pharmacother, 2014. **68**(8): p. 1049-56.
91. Zhang, X., et al., *A novel protoapigenone analog RY10-4 induces breast cancer MCF-7 cell death through autophagy via the Akt/mTOR pathway.* Toxicol Appl Pharmacol, 2013. **270**(2): p. 122-8.
92. Yuan, Q., et al., *A new protoapigenone analog RY10-4 induces apoptosis and suppresses invasion through the PI3K/Akt pathway in human breast cancer.* Cancer Lett, 2012. **324**(2): p. 210-20.
93. Xue, P., et al., *A novel protoapigenone analog RY10-4 induces apoptosis of breast cancer cells by exacerbating mitochondrial Ca(2+) influx through mitochondrial calcium uniporter.* Toxicol Appl Pharmacol, 2021. **433**: p. 115776.
94. Liu, Z., et al., *RY10-4, a novel anti-tumor compound, exhibited its anti-angiogenesis activity by down-regulation of the HIF-1α and inhibition phosphorylation of AKT and mTOR.* Cancer Chemother Pharmacol, 2012. **69**(6): p. 1633-40.
95. Liu, Z., et al., *RY10-4 suppressed metastasis of MDA-MB-231 by stabilizing ECM and E-cadherin.* Biomed Pharmacother, 2014. **68**(4): p. 439-45.
96. Xue, P., et al., *A novel compound RY10-4 induces apoptosis and inhibits invasion via inhibiting STAT3 through ERK-, p38-dependent pathways in human lung adenocarcinoma A549 cells.* Chem Biol Interact, 2014. **209**: p. 25-34.
97. Homayoonfal, M., Z. Asemi, and B. Yousefi, *Potential anticancer properties and mechanisms of thymoquinone in osteosarcoma and bone metastasis.* Cell Mol Biol Lett, 2022. **27**(1): p. 21.
98. Ahmad, A., et al., *A review on therapeutic potential of Nigella sativa: A miracle herb.* Asian Pac J Trop Biomed, 2013. **3**(5): p. 337-52.
99. Jehan, S., et al., *Combinatorial effect of thymoquinone with chemo agents for tumor therapy.* Phytomedicine, 2022. **98**: p. 153936.
100. Adinew, G.M., et al., *Therapeutic Potential of Thymoquinone in Triple-Negative Breast Cancer Prevention and Progression through the Modulation of the Tumor Microenvironment.* Nutrients, 2021. **14**(1).
101. Akin, A.T., et al., *Therapeutic effects of thymoquinone in doxorubicin-induced hepatotoxicity via oxidative stress, inflammation and apoptosis.* Anat Histol Embryol, 2021. **50**(6): p. 908-917.
102. Al-Rawashde, F.A., et al., *Thymoquinone Inhibits Growth of Acute Myeloid Leukemia Cells through Reversal SHP-1 and SOCS-3 Hypermethylation: In Vitro and In Silico Evaluation.* Pharmaceuticals, 2021. **14**(12): p. 1287.
103. Chowdhury, F.A., et al., *Therapeutic Potential of Thymoquinone in Glioblastoma Treatment: Targeting Major Gliomagenesis Signaling Pathways.* Biomed Res Int, 2018. **2018**: p. 4010629.
104. Dalli, M., et al., *Nigella sativa L. Phytochemistry and Pharmacological Activities: A Review (2019-2021).* Biomolecules, 2021. **12**(1): p. 20.
105. Kaymak, E., et al., *Thymoquinone has a neuroprotective effect against inflammation, oxidative stress, and endoplasmic reticulum stress in the brain cortex, medulla, and hippocampus due to doxorubicin.* J Biochem Mol Toxicol, 2021. **35**(11): p. e22888.
106. Malik, S., et al., *Thymoquinone: A small molecule from nature with high therapeutic potential.* Drug Discov Today, 2021. **26**(11): p. 2716-2725.
107. Phua, C.Y.H., et al., *Triangulating the pharmacological properties of thymoquinone in regulating reactive oxygen species, inflammation, and cancer: Therapeutic applications and mechanistic pathways.* Life Sci, 2021. **287**: p. 120120.

108. Taysi, S., et al., *Thymoquinone: A Review of Pharmacological Importance, Oxidative Stress, COVID-19, and Radiotherapy.* Mini Rev Med Chem, 2022. **22**(14): p. 1847-1875.
109. Woo, C.C., et al., *Anticancer activity of thymoquinone in breast cancer cells: possible involvement of PPAR-γ pathway.* Biochem Pharmacol, 2011. **82**(5): p. 464-75.
110. Farooq, J., et al., *Insights into the Protective Effects of Thymoquinone against Toxicities Induced by Chemotherapeutic Agents.* Molecules, 2021. **27**(1): p. 226.
111. Al Bitar, S., et al., *Thymoquinone Radiosensitizes Human Colorectal Cancer Cells in 2D and 3D Culture Models.* Cancers, 2022. **14**(6): p. 1363.
112. Park, E.J., et al., *Thymoquinone induces apoptosis through downregulation of c-FLIP and Bcl-2 in renal carcinoma Caki cells.* Oncol Rep, 2016. **36**(4): p. 2261-7.
113. Gurung, R.L., et al., *Thymoquinone induces telomere shortening, DNA damage and apoptosis in human glioblastoma cells.* PLoS One, 2010. **5**(8): p. e12124.
114. El-Najjar, N., et al., *Reactive oxygen species mediate thymoquinone-induced apoptosis and activate ERK and JNK signaling.* Apoptosis, 2010. **15**(2): p. 183-95.
115. Homayoonfal, M., Z. Asemi, and B. Yousefi, *Targeting microRNAs with thymoquinone: a new approach for cancer therapy.* Cell Mol Biol Lett, 2021. **26**(1): p. 43.
116. Karim, S., et al., *PI3K-AKT Pathway Modulation by Thymoquinone Limits Tumor Growth and Glycolytic Metabolism in Colorectal Cancer.* Int J Mol Sci, 2022. **23**(4): p. 2305.
117. Al-Rawashde, F.A., et al., *Thymoquinone Induces Downregulation of BCR-ABL/JAK/STAT Pathway and Apoptosis in K562 Leukemia Cells.* Asian Pac J Cancer Prev, 2021. **22**(12): p. 3959-3965.
118. El-Far, A.H., et al., *Thymoquinone and Costunolide Induce Apoptosis of Both Proliferative and Doxorubicin-Induced-Senescent Colon and Breast Cancer Cells.* Integr Cancer Ther, 2021. **20**: p. 15347354211035450.
119. Abd-Rabou, A.A., et al., *Thymoquinone Crosstalks with DR5 to Sensitize TRAIL Resistance and Stimulate ROS-Mediated Cancer Apoptosis.* Asian Pac J Cancer Prev, 2021. **22**(9): p. 2855-2865.
120. Narayanan, P., et al., *Natural quinones induce ROS-mediated apoptosis and inhibit cell migration in PANC-1 human pancreatic cancer cell line.* J Biochem Mol Toxicol, 2022. **36**(5): p. e23008.
121. Krylova, N.G., et al., *Cytotoxic and antiproliferative effects of thymoquinone on rat C6 glioma cells depend on oxidative stress.* Mol Cell Biochem, 2019. **462**(1-2): p. 195-206.
122. Racoma, I.O., et al., *Thymoquinone inhibits autophagy and induces cathepsin-mediated, caspase-independent cell death in glioblastoma cells.* PLoS One, 2013. **8**(9): p. e72882.
123. Kolli-Bouhafs, K., et al., *Thymoquinone reduces migration and invasion of human glioblastoma cells associated with FAK, MMP-2 and MMP-9 down-regulation.* Invest New Drugs, 2012. **30**(6): p. 2121-31.
124. Pazhouhi, M., et al., *Thymoquinone synergistically potentiates temozolomide cytotoxicity through the inhibition of autophagy in U87MG cell line.* Iran J Basic Med Sci, 2016. **19**(8): p. 890-898.
125. Khazaei, M. and M. Pazhouhi, *Temozolomide-Mediated Apoptotic Death Is Improved by Thymoquinone in U87MG Cell Line.* Cancer Invest, 2017. **35**(4): p. 225-236.
126. Mai, A., et al., *Thymoquinone induces apoptosis in temozolomide-resistant glioblastoma cells via the p38 mitogen-activated protein kinase signaling pathway.* Environ Toxicol, 2022. **38**(1): p. 90-100.
127. Wei, C., et al., *TQFL12, a novel synthetic derivative of TQ, inhibits triple-negative breast cancer metastasis and invasion through activating AMPK/ACC pathway.* J Cell Mol Med, 2021. **25**(21): p. 10101-10110.
128. Ivasiv, V., et al., *Molecular Hybridization as a Tool for Designing Multitarget Drug Candidates for Complex Diseases.* Curr Top Med Chem, 2019. **19**(19): p. 1694-1711.

129. de Oliveira Pedrosa, M., et al., *Hybrid Compounds as Direct Multitarget Ligands: A Review.* Curr Top Med Chem, 2017. **17**(9): p. 1044-1079.
130. Abdolmaleki, A. and J.B. Ghasemi, *Dual-acting of Hybrid Compounds - A New Dawn in the Discovery of Multi-target Drugs: Lead Generation Approaches.* Curr Top Med Chem, 2017. **17**(9): p. 1096-1114.
131. Tietze, L.F., H.P. Bell, and S. Chandrasekhar, *Natural product hybrids as new leads for drug discovery.* Angew Chem Int Ed Engl, 2003. **42**(34): p. 3996-4028.
132. Reiter, C., et al., *New artesunic acid homodimers: potent reversal agents of multidrug resistance in leukemia cells.* Bioorg Med Chem, 2012. **20**(18): p. 5637-5641.
133. Fröhlich, T., et al., *Artemisinin-Derived Dimers: Potent Antimalarial and Anticancer Agents.* J Med Chem, 2016. **59**(16): p. 7360-88.
134. Latif, A.D., et al., *Protoflavone-Chalcone Hybrids Exhibit Enhanced Antitumor Action through Modulating Redox Balance, Depolarizing the Mitochondrial Membrane, and Inhibiting ATR-Dependent Signaling.* Antioxidants, 2020. **9**(6): p. 519.
135. Girst, G., et al., *Hybrid molecules of protoflavones and spirooxindole derivatives with selective cytotoxicity against triple-negative breast cancer cells.* RSC Med Chem, 2023. 14: p. 1778-1786.
136. Ndreshkjana, B., et al., *Combination of 5-fluorouracil and thymoquinone targets stem cell gene signature in colorectal cancer cells.* Cell Death Dis, 2019. **10**(6): p. 379.
137. Fröhlich, T., et al., *Synthesis of Novel Hybrids of Thymoquinone and Artemisinin with High Activity and Selectivity Against Colon Cancer.* ChemMedChem, 2017. **12**(3): p. 226-234.
138. Wei, C.K., et al., *6-Paradol and 6-Shogaol, the Pungent Compounds of Ginger, Promote Glucose Utilization in Adipocytes and Myotubes, and 6-Paradol Reduces Blood Glucose in High-Fat Diet-Fed Mice.* Int J Mol Sci, 2017. **18**(1).
139. Yao, J., et al., *Activation of the phase II enzymes for neuroprotection by ginger active constituent 6-dehydrogingerdione in PC12 cells.* J Agric Food Chem, 2014. **62**(24): p. 5507-18.
140. Kumboonma, P., et al., *Identification of phenolic compounds from Zingiber offinale and their derivatives as histone deacetylase inhibitors and antioxidants.* Med Chem Res, 2017. **26**: p. 650-661.
141. Murphree, S.S., et al., *Rapid Aqueous Borohydride Reduction of Carbonyls Under Sealed-Tube Microwave Conditions.* Synthetic Communications, 2012. **42**(13): p. 1979-1986.
142. Balaji, N.V., et al., *Design, synthesis and in vitro cell-based evaluation of the anti-cancer activities of hispolon analogs.* Bioorg Med Chem, 2015. **23**(9): p. 2148-2158.
143. Szakonyi, Z., et al., *Stereoselective syntheses and transformations of chiral 1,3-aminoalcohols and 1,3-diols derived from nopinone.* Tetrahedron: Asymmetry, 2014. **25**(15): p. 1138-1145.
144. Lin, Y.T., et al., *Discovery of 7, 4'-dimethoxy-3-hydroxyflavone as a protease-activated receptor 4 antagonist with antithrombotic activity and less bleeding tendency in mice.* Biochem Pharmacol, 2022. **202**: p. 115152.
145. *ACD/Labs Percepta*. [Version: v2021.2.1. Build 3525] ; Available from: https://www.acdlabs.com/products/percepta/
146. *Marvin Sketch, Tautomer Generator*. Chemaxon.
147. Avdeef, A., *Permeability Equations*, in *Absorption and Drug Development: Solubility, Permeability, and Charge State*. 2012, Wiley Interscience: Hoboken, NJ, USA. p. 465–481.
148. Fukumoto, L.R. and G. Mazza, *Assessing antioxidant and prooxidant activities of phenolic compounds.* J Agric Food Chem, 2000. **48**(8): p. 3597-604.
149. Mielnik, M.B., et al., *Antioxidant and other quality properties of reindeer muscle from two different Norwegian regions.* Meat Sci, 2011. **89**(4): p. 526-32.
150. Fási, L., et al., *AAPH or Peroxynitrite-Induced Biorelevant Oxidation of Methyl Caffeate Yields a Potent Antitumor Metabolite.* Biomolecules, 2020. **10**(11): p. 1537.
151. Morris, G.M., et al., *AutoDock4 and AutoDockTools4: Automated docking with selective receptor flexibility.* J Comput Chem, 2009. **30**(16): p. 2785-91.

152. Tóth, L., L. Muszbek, and I. Komáromi, *Mechanism of the irreversible inhibition of human cyclooxygenase-1 by aspirin as predicted by QM/MM calculations.* J Mol Graph Model, 2013. **40**: p. 99-109.
153. O'Boyle, N.M., et al., *Open Babel: An open chemical toolbox.* J Cheminformatics, 2011. **3**(1): p. 33.
154. Redden, P.R., et al., *Acyloxymethyl acidic drug derivatives: in vitro hydrolytic reactivity.* Int Journal Pharm, 1999. **180**(2): p. 151-160.
155. Mosmann, T., *Rapid colorimetric assay for cellular growth and survival: application to proliferation and cytotoxicity assays.* J Immunol Methods, 1983. **65**(1-2): p. 55-63.
156. Wager, T.T., et al., *Central Nervous System Multiparameter Optimization Desirability: Application in Drug Discovery.* ACS Chem Neurosci, 2016. **7**(6): p. 767-775.
157. Asakawa, Y., et al., *Efficient preparation of some biologically active substances from natural and nonnatural aromatic compounds by m-chloroperbenzoic acid oxidation.* J Org Chem, 1988. **53**(23): p. 5453-5457.
158. Semwal, R.B., et al., *Gingerols and shogaols: Important nutraceutical principles from ginger.* Phytochem, 2015. **117**: p. 554-568.
159. Badimon, L., et al., *The key contribution of platelet and vascular arachidonic acid metabolism to the pathophysiology of atherothrombosis.* Cardiovasc Res, 2021. **117**(9): p. 2001-2015.
160. Leeson, P.D. and B. Springthorpe, *The influence of drug-like concepts on decision-making in medicinal chemistry.* Nat Rev Drug Discov, 2007. **6**(11): p. 881-890.
161. Edwards, M.P. and D.A. Price, *Chapter 23 - Role of Physicochemical Properties and Ligand Lipophilicity Efficiency in Addressing Drug Safety Risks*, in *Annual Reports in Medicinal Chemistry*, J.E. Macor, Editor. 2010, Academic Press. p. 380-391.
162. Nurtjahja-Tjendraputra, E., et al., *Effective anti-platelet and COX-1 enzyme inhibitors from pungent constituents of ginger.* Thromb Res, 2003. **111**(4-5): p. 259-65.
163. Ghazanfari, N., et al., *Is cyclooxygenase-1 involved in neuroinflammation?.* J Neurosci Res, 2021. **99**(11): p. 2976-2998.
164. Woodling, N.S., et al., *Cyclooxygenase inhibition targets neurons to prevent early behavioural decline in Alzheimer's disease model mice.* Brain, 2016. **139**(7): p. 2063-2081.
165. Aïd, S. and F. Bosetti, *Targeting cyclooxygenases-1 and -2 in neuroinflammation: Therapeutic implications.* Biochim, 2011. **93**(1): p. 46-51.
166. Guragossian, N., et al., *Candidate Molecule Selection Based on In Silico Predicted ADMET Properties of 12 Indenoindole Derivatives.* Chem Inform, 2016. **2**((2)6).
167. Lipinski, C.A., et al., *Experimental and computational approaches to estimate solubility and permeability in drug discovery and development settings1PII of original article: S0169-409X(96)00423-1. The article was originally published in Advanced Drug Delivery Reviews 23 (1997) 3–25.1.* Adv Drug Deliv Rev, 2001. **46**(1): p. 3-26.
168. Tinworth, C.P. and R.J. Young, *Facts, Patterns, and Principles in Drug Discovery: Appraising the Rule of 5 with Measured Physicochemical Data.* J Med Chem, 2020. **63**(18): p. 10091-10108.
169. Veber, D.F., et al., *Molecular Properties That Influence the Oral Bioavailability of Drug Candidates.* J Med Chem, 2002. **45**(12): p. 2615-2623.
170. Alsahli, M.A., et al., *6-Gingerol, a Major Ingredient of Ginger Attenuates Diethylnitrosamine-Induced Liver Injury in Rats through the Modulation of Oxidative Stress and Anti-Inflammatory Activity.* Mediators Inflamm, 2021. **2021**: p. 6661937.
171. Alharbi, K.S., et al., *Gingerol, a Natural Antioxidant, Attenuates Hyperglycemia and Downstream Complications.* Metabolites, 2022. **12**(12): p. 1274.
172. Forman, H.J. and H. Zhang, *Targeting oxidative stress in disease: promise and limitations of antioxidant therapy.* Nat Rev Drug Discov, 2021. **20**(9): p. 689-709.
173. Tiruppur Venkatachallam, S.K., et al., *Chemical composition of Nigella sativa L. seed extracts obtained by supercritical carbon dioxide.* J Food Sci Technol, 2010. **47**(6): p. 598-605.

174. Effenberger, K., S. Breyer, and R. Schobert, *Terpene conjugates of the Nigella sativa seed-oil constituent thymoquinone with enhanced efficacy in cancer cells.* Chem Biodivers, 2010. **7**(1): p. 129-39.
175. Yang, R., et al., *Therapeutic progress and challenges for triple negative breast cancer: targeted therapy and immunotherapy.* Mol Biomed, 2022. **3**(1): p. 8.
176. Sun, X., et al., *BRD8 maintains glioblastoma by epigenetic reprogramming of the p53 network.* Nature, 2023. **613**(7942): p. 195-202.
177. Majd, N.K., et al., *The promise of DNA damage response inhibitors for the treatment of glioblastoma.* Neuro-oncol Adv, 2021. **3**(1).

ACKNOWLEDGEMENTS

I am grateful to my supervisor, Dr. Attila Hunyadi for offering me a place among his team and supporting me during my PhD study. My sincere gratitude is due to Dr. Tímea Gonda for the very appreciated help and support I received from her. I am also grateful to Prof. Dr. Judit Hohmann, Head of the Doctoral School of Pharmaceutical Sciences for kindly accepting me to join this program and for supporting all of us during this journey.

I am thankful to Dr. Norbert Kúsz, Dr. Kornél Szőri, Gábor Girst for the NMR measurements, Dr. Róbert Berkecz for the MS measurements, Bizhar A. Tayeb, Dr. Renáta Minorics, Prof. István Zupkó, Meng-Chun Tsai, and Prof. Chin-Chung Wu for the bioactivity testing, Orinamhe Agbadua and Gábor Girst for the enzymatic assays, and Prof. György T. Balogh for performing the pharmacokinetic and *in silico* ADME studies.

Many thanks to my colleagues in the group, without their help it wouldn't have been possible to achieve this. My thanks are likewise to Ibolya Hevérné Herke and Konrád Kurunczi-Papp for their help in research-related issues. I am very appreciative to my friends and all members of the Institute of Pharmacognosy for the great time and unique experience I had with them. I am thankful to anyone who helped me in one way or another during my PhD.

I do acknowledge the funding bodies: the National Research, Development and Innovation Office, Hungary (NKFIH; K134704), and TKP2021-EGA-32, implemented with the support provided by the Ministry of Innovation and Technology of Hungary from the NKFIH, financed under the TKP2021-EGA funding scheme. I am also thankful to the Tempus Public Foundation for offering me the scholarship and to the Faculty of Pharmacy, University of Khartoum, and the Ministry of Higher Education, Khartoum, Sudan for the financial support.

Last, but not the least, I am extremely indebted to my beloved mother who gave up her dreams for ours to come true, my siblings, my teachers, and my friends who stand by, day by day, moment by moment, very patiently and unconditionally supporting me throughout this journey.